The Isotope Geochemistry of Ni

Tim Elliott
tim.elliott@bristol.ac.uk
Bristol Isotope Group, School of Earth Sciences
University of Bristol
Bristol, BS8 1RJ, UK

Robert C. J. Steele
r.steele@uclmail.net
Institute for Geochemistry and Petrology
ETH Zürich
Zürich, 8092, Switzerland

1. INTRODUCTION

Nickel is an iron-peak element with 5 stable isotopes (see Table 1) which is both cosmochemically abundant and rich in the information carried in its isotopic signature. Significantly, ^{60}Ni is the radiogenic daughter of ^{60}Fe, a short-lived nuclide ($t_{1/2}$ = 2.62Ma; Rugel et al., 2009) of a major element. ^{60}Fe has the potential to be both an important heat source and chronometer in the early solar system. ^{60}Ni abundances serve to document the prior importance ^{60}Fe and this is a topic of on-going debate (section 3). The four other stable Ni nuclides span a sizeable relative mass range of ~10%, including the notably neutron-rich nuclide ^{64}Ni. The relative abundances of these isotopes vary with diverse stellar formation environments and provide a valuable record of the nucleosynthetic heritage of Ni in the solar system (section 2). Ni occurs widely as both elemental and divalent cationic species, substituting for Fe and Mg in common silicate structures and forming Fe/Ni metal alloys. The Ni isotope chemistry of all the major planetary reservoirs and fractionations between them can thus be characterised (section 4). Ni is also a bio-essential element and its fractionation during low-temperature biogeochemical cycling is a topic that has attracted recent attention (section 4).

1.1 Notation

Much of the work into Ni has been cosmochemical, focussing on the nucleosynthetic origins of different meteoritic components. Such studies have primarily investigated mass-independent isotopic variations, both radiogenic and non-radiogenic, which require choosing a reference isotope pair for normalisation. Throughout this work we use ^{58}Ni-^{61}Ni as the normalising pair, in keeping with current practice in the field. An alternative ^{58}Ni-^{62}Ni normalisation scheme has previously been used for bulk analyses (Shimamura and Lugmair 1983; Shukolyukov and Lugmair, 1993a,b; Cook et al., 2007; Cook et al., 2008; Quitté et al., 2006; Quitté et al., 2011; Chen et al., 2009) and one early study used ^{58}Ni-^{60}Ni (Morand and Allègre, 1983). Although the large isotopic variability accessible by *in situ* analyses often makes external normalisation a viable option for mass-independent measurements by secondary ionisation mass-spectrometry (SIMS), some have employed internal normalisation in determinations of ^{60}Ni/^{61}Ni (Tachibana and Huss, 2003; Tachibana et al., 2006; Mishra and Chaussidon, 2014; Mishra et al., 2016). Given unresolvable Fe and Zn interferences on masses 58 and 64, this requires normalising to ^{62}Ni/^{61}Ni. In this review, all data have been renormalised to ^{58}Ni-^{61}Ni, where possible. Some studies have only reported normalised data and so such conversion cannot be made. Fortunately, the subtle differences resulting from different normalisations do not affect the inferences being made in these cases and we simply indicate the normalisation scheme used. To be clear about these potentially important details, we use a notation proposed by Steele et al. (2011), which includes this information. For example:

$$\varepsilon^{60}Ni_{58/61} = (^{60}Ni/^{58}Ni^{sample}{}_{norm\ 58/61} / ^{60}Ni/^{58}Ni^{standard}{}_{norm\ 58/61} - 1) \times 10000 \qquad \text{(Eq 1)}$$

or the parts per ten thousand variation of $^{60}Ni/^{58}Ni$ (internally normalised to a reference $^{58}Ni/^{61}Ni$) relative to a standard measured in the same way. The established isotopic standard for Ni is the National Institute of Standards and Technology Standard Reference Material (NIST SRM) 986, Gramlich et al. (1989). Reference Ni isotope ratios for this standard are reported in Table 1. This NIST SRM has been widely used, providing a valuable common datum in all but the earliest work. If it is necessary to clarify which reference standard has been used, the notation above can be augmented, e.g. $\varepsilon^{60}Ni_{58/61}$ (NIST 986). For elements such as Ni, however, where the same standard is conventionally used, we feel this additional information can be omitted without too much confusion, provided it is imparted elsewhere (as we do here). We use the epsilon notation solely for mass-independent isotopic data (internally normalised). This approach is typical although not universal and the presence of the subscript in our notation (Eq 1) makes the use of internal normalisation evident.

We report mass-dependent variations in the delta notation:

$$\delta^{60/58}Ni = (^{60}Ni/^{58}Ni^{sample} / ^{60}Ni/^{58}Ni^{standard} - 1) \times 1000 \qquad \text{(Eq 2)}$$

As for the mass-independent work, NIST SRM 986 is extensively used as the Ni isotope reference standard and is implicit in Eq (2). In Eq (2), we follow another proposal made in Steele et al. (2011) to report the isotope ratio used, i.e. $\delta^{60/58}Ni$ instead of $\delta^{60}Ni$. This removes any ambiguity over which nuclide is used as the denominator. For an element such as Ni, with more than two stable isotopes, such qualification is valuable. We suggest this systematic notion could be useful more generally.

Moynier et al. (2007) reported their mass-dependent Ni isotope data as $\overline{\delta}Ni$, an error weighted, average fractionation per unit mass difference, using the three measured ratios $(^{60}Ni/^{58}Ni)/2$, $(^{61}Ni/^{58}Ni)/3$ and $(^{62}Ni/^{58}Ni)/4$. This is an interesting idea (see also Albalat et al., 2012), which reduces the error for the sample-standard bracketing technique by using all measured data. The alternative method for determining mass-dependent isotopic fractionation is by double-spiking (see review by Rudge et al., 2009). Double-spiking requires measurements of four isotopes, thus yielding three independent isotope ratio determinations. Given a troublesome Zn interference on mass 64, all double-spiked studies to date have used a ^{61}Ni-^{62}Ni double spike and employed ^{58}Ni, ^{60}Ni, ^{61}Ni and ^{62}Ni in the data reduction. With ostensible similarity to the sample-standard bracketing approach of Moynier et al. (2007), the combined measurements of these four isotopes yield a single value of natural isotopic fractionation, which is normally converted into a more tangible delta value for a specific but arbitrary isotope ratio (e.g. $\delta^{60/58}Ni$). The key difference in double-spiking is that the additional isotope ratios are used to constrain explicitly instrumental mass-bias. Namely this procedure improves accuracy, whereas in sample-standard bracketing instrumental mass bias is assumed to be identical for sample and standard and the additional isotope measurements are used to improve precision.

Both methods described above use measurements of ^{60}Ni for determining mass-dependent Ni isotope variability. It is germane to consider whether or not it makes good sense to use a radiogenic isotope for such a purpose. For terrestrial samples, there should be no variability in the relative abundance of radiogenic ^{60}Ni, given likely terrestrial isotopic homogenisation after parental ^{60}Fe became extinct. For extra-terrestrial samples, this is potentially a consideration, but bulk variations in $\varepsilon^{60}Ni_{58/61}$ are typically small (~0.1), dominantly nucleosynthetic rather than radiogenic and associated with mass-independent variability of other isotopes (see section 2). For the most accurate mass-dependent measurements, a second mass-independent isotopic determination is therefore required (e.g. Steele et al., 2012), but such mass-independent

variability does not have a significant impact on more typical mass-dependent determinations at the delta unit level (section 4.1).

In section 3 we address the presence of ^{60}Fe in the early solar system from ^{60}Ni measurements of meteoritic samples. Such determinations yield initial ^{60}Fe/^{56}Fe for the objects analysed, denoted ^{60}Fe/^{56}Fe°. Given samples that yield precise values of ^{60}Fe/^{56}Fe° may have different ages, it is useful to calculate ^{60}Fe/^{56}Fe° at a common reference time, typically the start of the solar system as marked by calcium aluminium rich inclusion formation. Such a solar system initial value is abbreviated to ^{60}Fe/^{56}Fe°$_{SSI}$. Throughout this review, the uncertainties quoted for various average measurements are two standard errors, unless otherwise stated.

2. NUCELOSYNTHETIC Ni ISOTOPIC VARIATIONS

Nickel is significant element in stellar nucleosynthesis. Nickel-62 has the highest binding energy per nucleon of any nuclide; no nuclear reaction involving heavier nuclides can produce more energy than it consumes. It is often, incorrectly, said that ^{56}Fe has the highest binding energy per nucleon, likely due to the anomalously high abundance of ^{56}Fe. In fact, ^{56}Fe is dominantly produced in stars as the decay product ^{56}Ni, which is the result of the last energetically favourable reaction during Si burning.

It is thought the Ni isotopes are dominantly produced during nuclear statistical equilibrium (NSE or the e-process) in supernovae (Burbidge, Burbidge Fowler and Hoyle 1957). There are two main astrophysical environments in which the majority of Ni is thought to be produced, these are the type Ia (SN Ia) and type II (SN II) supernovae. SN Ia are thought to be the violent explosions of carbon-oxygen white dwarves which accrete material from a binary host to reach the Chandrasekher limit (<1.39 $M_{\odot}$ non-rotating). SN Ia are highly neutron enriched environments and have been hypothesized to be the source of some important neutron-rich nuclides, including ^{48}Ca, ^{60}Fe, ^{62}Ni and ^{64}Ni. Due to the size of the progenitor (<1.39 $M_{\odot}$) the stars are old, ~1 Ga, as they have burned their fuel slowly. This means they out-live the stellar nurseries (lifetime ~10 Ma) in which they formed. Therefore, they would make an unlikely, and so very interesting, source for isotope anomalies in the Solar System. SNII are the terminal explosions of much larger stars (>12 $M_{\odot}$) which consequently have much shorter main sequence lifetimes. Their shorter lifetimes make them much more likely to return material to star forming regions, meaning they are a more probable source for nucleosynthetic anomalies in the Solar System.

Trying to identify nucleosynthetic contributions from specific stellar events, such as those described above, within the average composition of the solar system is very difficult. However, the presence of 'isotopic anomalies' within meteoritic material provides opportunities to try to fingerprint individual sources. Isotopic anomalies are mass-independent isotopic compositions that differ from anthropocentric terrestrial values, and can indicate a different blend nucleosynthetic products to those on Earth. Such heterogeneities reveal either imperfect mixing of contrasting stellar inputs to the solar system (e.g. Reynolds, 1960), or else the unmixing of components in a generally well mixed, but locally heterogeneous nebula (e.g. Trinquier et al., 2009). These observations are of great interest to understanding the processes occurring in the early solar nebula and the stellar contributors to our solar system.

Calcium aluminium rich inclusions (CAIs), found in some primitive meteorites, document isotopic anomalies in the elements hosted in the refractory minerals from which they are formed. This was initially evident in the mass-independent oxygen isotopic compositions (Clayton et al., 1973) of the abundant CAIs in the meteorite Allende, although this signature is now largely attributed to gas-phase processes in the nebula (e.g. Yurimoto and Kuramoto, 2004). However, isotopic anomalies were also discovered for a range of refractory metals (e.g. McCulloch and Wasserburg, 1978 a, b) which are still believed to document, at the macroscopic scale (>1mm),

nucleosynthetic mixtures that contrast with the bulk solar system. Following reports of mass-independent variations of other iron-peak nuclides (e.g. Lee et al., 1978; Heydegger et al., 1979), the first Ni isotopic analyses of Allende CAIs (Morand and Allègre, 1983; Shimamura and Lugmair, 1983) failed to resolve signatures that differed from terrestrial values, in all but a single, highly anomalous 'FUN' inclusion (Shimamura and Lugmair, 1983). Subsequent improvements in precision allowed Birck and Lugmair (1988) to resolve excesses of ~1 $\varepsilon^{62}Ni_{61/58}$ and ~3 $\varepsilon^{64}Ni_{61/58}$ within Allende CAIs (Fig. 1), which they noted was in keeping with a neutron-rich, equilibrium process nucleosynthesis. These findings were pleasingly compatible with anomalies in neutron-rich isotopes of Ca (Jungck et al., 1984) and Ti (Heydegger et al, 1979; Niederer et al., 1980; Niemeyer and Lugmair, 1981) from previous studies and excesses of ^{54}Cr in their own work (Birck and Lugmair, 1988). This landmark contribution identified the key mass-independent variations in Ni isotopes that would subsequently become apparent in bulk meteorite analyses.

The CAIs analysed by Birck and Lugmair (1988) also displayed ^{60}Ni enrichments, $\varepsilon^{60}Ni_{61/58}$ ~1 (Fig. 1a), potentially related to the decay of ^{60}Fe co-produced with the neutron-rich Ni isotopes (see section 3). If these $\varepsilon^{60}Ni_{61/58}$ values are taken solely as the consequence of *in situ* ^{60}Fe decay, they imply initial $^{60}Fe/^{56}Fe$ ~$1x10^{-6}$, but Birck and Lugmair (1988) cautioned against such an inference, given associated nucleosynthetic variations of comparable magnitude. Further analyses of CAIs by Quitté et al. (2007) similarly showed positive $\varepsilon^{60}Ni_{61/58}$ and $\varepsilon^{62}Ni_{61/58}$ (see Fig 1a); the method used in this study suffered from too large ^{64}Zn interferences to make precise $\varepsilon^{64}Ni_{61/58}$ measurements. The authors attributed their observations to synthesis of ^{60}Fe and ^{62}Ni (and ^{96}Zr) in a neutron burst event, followed by the decay of ^{60}Fe. Birck and Lugmair (1988) had argued against this style of model, given the absence of predicted, associated ^{46}Ca anomalies in CAIs. However, Quitté et al. (2007) tentatively inferred $^{60}Fe/^{56}Fe°_{SSI}$ >$1x10^{-6}$ from their nucleosynthetic model, a two point internal CAI isochron and the interpretation of $\varepsilon^{60}Ni_{61/58}$ excesses in two CAIs without $\varepsilon^{62}Ni_{61/58}$ anomalies.

Better precision was required to investigate mass-independent Ni isotopic variability between bulk meteorite samples. This came with improvements in mass-spectrometry, including multi-collection systems and their coupling with plasma sources (MC-ICPMS). The latter allows intense beams to be runs with relative ease, permitting counting statistical limitations to be overcome given sufficient sample availability. Nonetheless, the technique does require careful monitoring of a wide range of potential sample and plasma related interferences that may be significant at high precision (see common interferences listed in Steele et al., 2011 and Gall et al., 2012). Some of the earlier MC-ICPMS studies focussed on iron meteorites or the metallic phases of iron-bearing chondrites (Cook et al., 2006; Quitté et al., 2006; Moynier et al., 2007; Dauphas et al., 2008). This approach usefully exploits the natural concentration of Ni in a form readily purified to provide sufficient material for high precision analysis. In comparison, work on silicate samples requires more involved separation of Ni from a wider range of elements, typically accomplished using the highly Ni-specific complexing agent dimethylglyoxime either in solvent extraction (e.g. Morand and Allegre, 1983; Shimamura and Lugmair, 1983), mobile phase (e.g. Wahlgreen et al. 1970; Victor, 1986; Steele et al., 2011; Gall et al., 2012, Chernonozhkin et al, 2015) or stationary phase of ion-chromatography (e.g. Quitté and Oberli, 2006; Cameron and Vance, 2011). Alternatively, cation chromatography using a mixed HCl-acetone eluent (Strelow et al 1971) has also been successfully used (e.g. Tang and Dauphas, 2012).

Initial MC-ICPMS studies on meteoritic metal phases (Cook et al., 2006; Quitté et al., 2006; Moynier et al., 2007; Dauphas et al., 2008) dominantly argued against Ni isotope anomalies in bulk meteorites (Figs. 1-3), as did Chen et al. (2009) for their multi-collector thermal ionisation mass-spectrometry (MC-TIMS) analyses (Fig. 3). As exceptions to these overall observations of bulk Ni isotope homogeneity, Quitté et al. (2006) reported correlated, negative values of $\varepsilon^{60}Ni_{61/58}$ and $\varepsilon^{62}Ni_{61/58}$ in many of the sulfide inclusions they analysed from iron meteorites (Fig. 2a). Subsequently, Cook et al. (2008) reported more modest anomalies in troilites from iron

meteorites (Fig. 2). Both studies argued for the preservation of a pre-solar component in these sulfide inclusions, although how this occurred mechanistically was problematic. The MC-TIMS work of Chen et al. (2009) provided a different measurement perspective. This study argued against resolvable differences in $\varepsilon^{60}Ni_{61/58}$ and $\varepsilon^{62}Ni_{61/58}$ in either bulk or sulfide samples, at a level of ±0.2ε and ±0.5ε respectively (Fig. 2a). Since then, no one has further pleaded for the case of anomalous sulfides and the original analyses seem likely to have been measurement artefacts. However, there has been on-going debate about the presence of Ni isotopic anomalies in bulk meteorites.

In striking contrast to the bulk meteorite analyses described above, Bizzarro et al. (2007) reported a dataset with near constant negative $\varepsilon^{60}Ni_{61/58}$ (and $\varepsilon^{62}Ni_{61/58}$) in differentiated meteorites but $\varepsilon^{60}Ni_{61/58}$ ~0 and positive $\varepsilon^{62}Ni_{61/58}$ in chondrites. These data were used to invoke a late super-nova injection of ^{60}Fe into the solar system. Subsequent studies were unable to reproduce these results (Dauphas et al., 2008; Regelous et al., 2008; Chen et al., 2009; Steele et al., 2011) and noted that the systematics of the Bizzarro et al. (2007) dataset were consistent with an interference on ^{61}Ni. In reporting the results of further analyses, Bizzarro et al. (2010) commented that their new data were inconsistent with Bizzarro et al. (2007) but agreed with the observations of Regelous et al. (2008). The data from Bizzarro et al. (2007) will thus not be further considered.

Regelous et al. (2008) presented bulk analyses of $\varepsilon^{60}Ni_{61/58}$ and $\varepsilon^{62}Ni_{61/58}$ on a suite of chondrites and iron meteorites with precisions of around ±0.02 ε and ±0.04 ε respectively. By making higher precision measurements, in part by pooling multiple repeats of the same sample and by examining a wider range of meteorites than earlier studies, Regelous et al. (2008) were able to resolve differences in bulk meteorite compositions (Fig. 3a). They illustrated that variablity between different chondrite groups is largely echoed by that in iron meteorites (Fig. 3a). Notably the IVB irons have Ni isotopic compositions similar to carbonaceous chondrites (positive $\varepsilon^{62}Ni_{61/58}$), whilst the other magmatic irons resemble ordinary chondrites (with negative $\varepsilon^{62}Ni_{61/58}$). As for a number of other isotopic systems, enstatite chondrites were largely within error of terrestrial values.

These observations were further refined at higher precision (Fig. 4a) and with the inclusion of $\varepsilon^{64}Ni_{61/58}$ data (Fig. 4b) by Steele et al. (2011, 2012) and Tang and Dauphas (2012, 2014). These data revealed a continuous, well defined array in $\varepsilon^{62}Ni_{61/58}$ vs $\varepsilon^{64}Ni_{61/58}$ from ordinary chondrites and most magmatic irons, through terrestrial values in EH chondrites to carbonaceous chondrites and IVB irons (Fig. 4b). This ordering of meteorite groups is the same as observed in the mass-independent isotopic compositions of other first row, transition elements (Trinquier et al., 2007, 2009). Although the total isotopic variability in Ni is smaller than for Ti or Cr, its notable strength it that both chondrites and iron meteorites can be analysed to high precision, allowing genetic associations to be made from bulk compositions of iron meteorites rather than from occasional oxygen-bearing inclusions they contain (e.g. Clayton et al., 1983). Strikingly, the bulk Ni isotope array in Figure 4b points towards the CAI values presented by Birck and Lugmair (2008), see Figure 1b. For the same arguments as made by Trinquier et al. (2009), however, the bulk meteorite array is not formed by simple mixing between a single bulk composition and CAI, which would created a strongly curved array (see Figure 5). Carbonaceous chondrites are enriched, relative to ordinary chondrites, in the same isotopic component that is manifest more strongly in CAIs. Yet, it is not addition of CAIs themselves that causes the trend in Figure 4b but presumably variable abundances of specific pre-solar grains in chondrite matrices (see Dauphas et al., 2010 and Qin et al., 2011 for the Cr isotope case).

The well-defined array in non-radiogenic isotopes (Fig. 4b) provides key constraints on the nucleosynethetic origins of this important nebular component. At face value it represents coupled enrichments in the neutron rich isotopes of $\varepsilon^{62}Ni_{61/58}$ and $\varepsilon^{64}Ni_{61/58}$. However, the 3:1 slope of the array (Fig. 4b) can also be reproduced by variable meteoritic values of $^{58}Ni/^{61}Ni$, the

normalising isotope ratio. Indeed, from high-precision mass-dependent isotopic measurements (see section 4), Steele et al. (2012) showed that variability in ^{58}Ni best explains all observations. This implies the source of this anomalous Ni is from the Si-S zone of a SNII. This contrasts with material from the O-Ne zone required to account for a similarly constrained component in the Ti isotopic system. Steele et al. (2012) suggested ways in which the different, contributing zones for these different elements might be reconciled by grains from different zones being sorted (homogenised or unmixed) by solar system processes. However, these issues remain unresolved.

The correlation of bulk analyses of $\varepsilon^{60}Ni_{61/58}$ with the other isotope ratios ($\varepsilon^{62}Ni_{61/58}$ or $\varepsilon^{64}Ni_{61/58}$) is much less systematic (Regelous et al., 2008; Steele et al., 2012; Tang and Dauphas, 2014), see Figure 4a. In general, carbonaceous chondrites have lower $\varepsilon^{60}Ni_{61/58}$ than ordinary chondrites and enstatite chondrites, but CI chondrites are a notable exception. It is tempting to attribute these different relationships to the radiogenic nature of $\varepsilon^{60}Ni_{61/58}$, but given the abundance of ^{60}Fe inferred from bulk meteorite studies (see section 3 below) this seems unlikely. Instead, this presumably reflects part of a more complex nucleosythetic signature, with several components, potentially one which incorporates high fossil ^{60}Fe, involved in generating the Ni isotopic compositions of ordinary and carbonaceous chondrites.

The carriers of the exotic Ni isotopic components that shape variable bulk meteorite compositions remain to be identified. The highly anomalous isotopic compositions found in separated SiC grains from the CM2 meteorite, Murchison (Marhas et al., 2008) do not readily account for the mass-independent Ni isotope variations seen in bulk samples. These ion-probe analyses show ^{61}Ni/^{58}Ni and ^{62}Ni/^{58}Ni ratios >1000ε higher than terrestrial values (for these extreme ratios there is no internal normalisation) in X-grains believed to be derived from SNII sources. These Ni isotopic signatures suggest derivation from outer He/N and He/C zones of an SNII event, different to those inferred by Steele et al. (2012) to be necessary to account for bulk isotopic variability. As with other analyses of pre-solar SiC, these measurements bear striking testimony to the diversity of stellar sources that contribute to the bulk composition of the solar system, but do not identify a carrier for the signature that causes variability between different bulk, meteoritic objects (Steele and Boehnke, 2016).

3. EXTINCT ^{60}Fe AND RADIOGENIC ^{60}Ni

As alluded to in the preceding section, much of the initial interest in Ni isotope cosmochemistry was focussed on trying to identify the presence of live ^{60}Fe in the early solar system. A salient property of ^{60}Fe is that it is only made during stellar nucleosynthesis and cannot be produced by particle irradiation in our own solar system, unlike ^{26}Al (Lee et al. 1998). Thus an initial solar system value of ^{60}Fe/^{56}Fe (^{60}Fe/^{56}Fe°$_{SSI}$) significantly higher than the calculated steady state background of the interstellar medium (ISM), recently estimated at ~3×10^{-7} by Tang and Dauphas (2012), would provide strong evidence for injection of short-lived nuclides by a proximal stellar explosion. Such an explanation, linked to a trigger for solar system formation, has long been invoked to account for the elevated initial solar system ^{26}Al/^{27}Al (e.g. Cameron and Turan, 1977), but alternative means of generating ^{26}Al (e.g. Clayton and Jin, 1995) have made a more definitive test using ^{60}Fe highly desirable (see Wasserburg et al., 1998). As explored below, values of ^{60}Fe/^{56}Fe°$_{SSI}$ determined from Ni isotopic measurements of meteorites, remain contentious although our own perspective is that values above those of the ISM are questionable.

In a pioneering contribution, Shukolyukov and Lugmair (1993a) reported evidence for live ^{60}Fe from analyses of ^{60}Ni/^{58}Ni on samples of the eucrite Chervony Kut. Eucrites represent a good target for detecting *in situ* decay of ^{60}Fe, given their extremely high Fe/Ni (>10000). Such high Fe/Ni ratios are a consequence of core formation at low pressures (i.e. on a small planetary body) and subsequent magmatic fractionation. Given the formation and differentiation of the

eucrite parent body within the first few million years of solar system history (e.g. Papanastassiou and Wasserburg, 1969) the resultant Fe/Ni were likely to generate resolvable ^{60}Ni anomalies given significant initial ^{60}Fe. Different components of Chervony Kut showed elevated $\varepsilon^{60}Ni_{62/58}$ (up to 50) and three bulk samples with a range of Fe/Ni defined a straight line with a slope that implied $^{60}Fe/^{56}Fe° \sim 4x10^{-9}$ (Fig. 6a). The authors used an age of 10±2 Ma post CAI, from the similarity of the meteorites' $^{87}Sr/^{86}Sr$ to dated angrites (Lugmair and Galer, 1992), to calculate $^{60}Fe/^{56}Fe°_{SSI} = 1.6x10^{-6}$. Since then, determinations of the timing of differentiation of the eucrite parent body give older ages, ~3Ma post CAI (Lugmair and Shukolyukov, 1998; Bizzarro et al. 2005: Trinquier et al., 2008; Schiller et al., 2010) and the accepted half-life of ^{60}Fe has increased from 1.49 Ma (Kutchera et al., 1984) to 2.62Ma (Rugel et al., 2009). As a result of these changes a more contemporary interpretation of these results would yield $^{60}Fe/^{56}Fe°_{SSI} \sim 9x10^{-9}$.

Shukolyukov and Lugmair (1993a) originally noted that their value of $^{60}Fe/^{56}Fe°_{SSI}$ was in keeping with $\varepsilon^{60}Ni_{62/58}$ measurements made on CAIs by Birck and Lugmair (1988), assuming that such ^{60}Ni excesses were radiogenic. From the discussion of nucleosynthetic variability in section 2, it should be clear that this assumption is by no means valid, nor is the value thus derived consistent with the revised $^{60}Fe/^{56}Fe°_{SSI}$. The magnitude of possibly radiogenic $\varepsilon^{60}Ni_{61/58}$ in CAIs is no bigger than $\varepsilon^{62}Ni_{61/58}$, which must be nucleosynthetic (Fig. 1a). Although Kruijier et al. (2014) demonstrated that it is possible to disentangle nucleosynthetic from radiogenic contributions to $^{182}W/^{184}W$ in CAIs in order to define $^{182}Hf/^{180}Hf°_{SSI}$, neither initial parent nor parent-daughter fractionation in CAIs are sufficiently large to make this approach viable for determining $^{60}Fe/^{56}Fe°_{SSI}$. Indeed, most CAIs have sub-chondritic $^{56}Fe/^{58}Ni$ (e.g. Quitté et al., 2007), as a result of the slightly more refractory cosmochemical behaviour of Ni relative to Fe. Thus at best, minor $\varepsilon^{60}Ni_{61/58}$ deficits in bulk CAI would be expected if $^{60}Fe/^{56}Fe°_{SSI}$ were large enough for the bulk nebula to evolve to more radiogenic $\varepsilon^{60}Ni_{61/58}$, as is the case for the ^{53}Mn-^{53}Cr system (Birck and Allègre, 1985). Moreover, internal CAI isochrons offer little scope for constraining $^{60}Fe/^{56}Fe°_{SSI}$ given both modest Fe/Ni fractionation between common phases in CAIs and the frequent disturbance of Fe/Ni ratios in CAIs specifically (Quitté et al., 2007) and chondritic meteorites in general (e.g. Telus et al., 2016). In contrast to the ^{26}Al-^{26}Mg and ^{182}Hf-^{182}W systems, but similar to the ^{53}Mn-^{53}Cr pair, CAIs therefore offer scant opportunity to determine the initial parent abundance of the ^{60}Fe-^{60}Ni system. Instead, basaltic achondrites, with their highly fractionated Fe-Ni, have been the focus of much additional work to constrain $^{60}Fe/^{56}Fe°_{SSI}$.

In a follow-on study, Shukolyukov and Lugmair (1993b) analysed the eucrite Juvinas and noted an order of magnitude lower $^{60}Fe/^{56}Fe°$ ($\sim 4x10^{-10}$), which the authors attributed to ~4 Ma evolution of the eucrite parent body mantle source between generation of the basaltic melts represented by Chervony Kut and Juvinas. Using the newer ^{60}Fe half-life this period would be ~9 Ma, a value which resonates with the age difference of ~11 Ma inferred from Hf-W analyses between a group of eucrites including Juvinas and an older group of eucrites (Touboul et al., 2015); sadly Chervony Kut itself was not analysed for its Hf-W systematics. As with Chervony Kut (Shukolyukov and Lugmair, 1993a), separated mineral phases from Juvinas did not show meaningful isochronous relations and Shukolyukov and Lugmair (1993b) argue that the mobility/diffusivity of Ni made it susceptible to resetting on this shorter length scale, especially given the complex history of eucrites, with well documented thermal metamorphism (e.g. Takeda and Graham, 1991).

Subsequent studies of eucrites have been made with increasingly precise analyses using MC-ICPMS, but in essence show comparable features. Quitté et al. (2011) reported data for Bouvante and further analyses of Juvinas. Whole rock sub-samples of Bouvante define two arrays and if these are taken to be isochrons they imply $^{60}Fe/^{56}Fe° = 5x10^{-9}$ (but with an implausibly negative intercept of $\varepsilon^{60}Ni_{62/58} = -24 \pm 3$) and $^{60}Fe/^{56}Fe° = 5x10^{-10}$ (with a reasonable, near zero $\varepsilon^{60}Ni_{62/58}$ intercept). Instead, the authors argue that the data represent two mixing lines between clasts of different compositions. Whilst the second array gives a similar value of

$^{60}Fe/^{56}Fe°$ to Juvinas, as obtained by Shukolyukov and Lugmair (1993b), additional measurements of Juvinas by Quitté et al. (2011) are inconsistent with the array of Shukolyukov and Lugmair (1993b). Quitté et al. (2011) obtain a higher $^{60}Fe/^{56}Fe°$ ($2x10^{-9}$), using their two unwashed bulk samples and two unwashed, lower Fe/Ni samples from the Shukolyukov and Lugmair (1993b) array (ignoring the washed samples which they argue may have suffered Fe-Ni fractionation as a result of this preparation). As with the work of Shukolyukov and Lugmair (1993b), the Juvinas mineral analyses of Quitté et al. (2011) are scattered and presumably perturbed by secondary processes. There is clear difficulty in distinguishing primary from secondary signatures in these brecciated, thermally metamorphosed meteorites, but none of the eucrite arrays define $^{60}Fe/^{56}Fe°$ greater than $4x10^{-9}$.

Tang and Dauphas (2012) comprehensively reassessed this issue using a collection of bulk eucrites and diogenites. This dataset gave a large range in Fe/Ni, which coupled with their high precision measurements (typical $\varepsilon^{60}Ni_{61/58}$ better than ±0.3), provided a more definitive $^{60}Fe/^{56}Fe°$ = (3.5±0.3)$x10^{-9}$ for the eucrite parent body. This result is notably in keeping with the higher values obtained from 'internal isochrons' on sub-samples of meteorites discussed above (e.g. Fig. 6a). Using an age of 2.4±1.1Ma post CAI for silicate differentiation of 4 Vesta (Trinquier et al., 2008; Connelly et al., 2012), which presumably sets the variable Fe/Ni seen in the eucrites, these data yield a $^{60}Fe/^{56}Fe°_{SSI}$ (6.6±2.5)$x10^{-9}$. This work of Tang and Dauphas (2012) also yields a bound of 4±2 Ma on the age of core formation on 4 Vesta, from a two-stage evolution model of the mantle. Namely, the $\varepsilon^{60}Ni_{61/58}$ of the mantle, determined by the intercept of the eucrite-diogenite array with an estimated bulk mantle $^{56}Fe/^{58}Ni \sim 2700$ informs on the time since core formation. Tang and Dauphas (2014) subsequently used a similar approach to constrain the timing of core formation and hence growth of Mars. They argued that the planet reached 44% of its size no earlier than 1.2Ma post CAI or otherwise the $\varepsilon^{60}Ni_{61/58}$ of the SNC meteorites they measured would be more radiogenic.

Quenched angrites provide a more petrologically robust sample for determining $^{60}Fe/^{56}Fe°$, even if their Fe/Ni are not quite as extreme as the eucrites (cf. Figs. 6a & b). Moreover, the well-defined ages for these samples determined using extant isotope chronometry (Amelin 2008a,b; Connolly et al., 2008, Brennecka and Wadhwa, 2012), potentially provide more accurate decay correction in calculating $^{60}Fe/^{56}Fe°_{SSI}$. Three independent studies (Quitté et al., 2010; Spivak-Birndorf et al., 2011; Tang and Dauphas 2012) obtained consistent values for internal isochrons of d'Orbigny (e.g. Fig. 6b) which give a weighted average $^{60}Fe/^{56}Fe°$ = (3.3±0.5)$x10^{-9}$. Two internal isochrons from a second quenched angrite, Sahara 99555, are also in mutual agreement but yield a lower weighted mean $^{60}Fe/^{56}Fe°$ = (1.9±0.4)$x10^{-9}$ (Quitté et al., 2010; Tang and Dauphas, 2015). Tang and Dauphas (2015) convincingly argue this difference relative to d'Orbigny likely reflects terrestrial weathering experienced by Sahara 99555.

In all, these angrite $^{60}Fe/^{56}Fe°$ are in keeping with those of eucrites, suggesting a similar initial ^{60}Fe and timing of planetary differentiation on these two bodies. So a reassuringly consistent value has emerged from these various TIMS/MC-ICPMS studies which span several decades of work. The data from d'Orbigny provides the best constrained value and using an age of 3.9Ma post CAI (Amelin 2008a; Brennecka and Wadhwa, 2012; Connelly et al., 2012) we calculate $^{60}Fe/^{56}Fe°_{SSI}$ =(9.8±4.5)$x10^{-9}$. We note this value is lower than the equivalent cited by Tang and Dauphas (2012) as a consequence of our using the Pb-Pb ages rather than Mn-Cr chronometry.

Further bulk analyses of a range of meteoritic materials are supportive of the low $^{60}Fe/^{56}Fe°_{SSI}$ determined from angrite and eucrite analyses, albeit from less well constrained scenarios. Shukolyukov and Lugmair (1993b) and Quitté et al. (2010) reported no systematic differences in $\varepsilon^{60}Ni_{62/58}$ for various bulk samples (ureilites) and separated phases (e.g. troilite) with high but variable Fe/Ni ratios. Moynier et al. (2011) placed a maximum upper bound on $^{60}Fe/^{56}Fe°_{SSI}$ of $3x10^{-9}$ from the absence of ^{60}Ni isotope anomalies in measurements of troilite

from the iron meteorite Muonionalusta. These troilites have Pb-Pb model ages as old as the quenched angrites (Blichert-Toft et al., 2010), which coupled with their high Fe/Ni (up to 1500) should result in radiogenic $\varepsilon^{60}Ni_{61/58}$ given sufficiently high $^{60}Fe/^{56}Fe°$. Although appealing targets for analysis, re-equilibration of the troilites with the surrounding Ni-rich metal during parent body during cooling would tend to erase any $\varepsilon^{60}Ni_{61/58}$ anomalies. The authors briefly argue against such an interpretation on the basis of the preservation of ancient Pb-Pb ages, but the potential for diffusional exchange of Ni with the Ni-rich host metal (see Chernonozhkin et al., 2016) seems much greater than for Pb. Whilst the conclusions of Moynier et al (2011) are thus compatible with other studies, whether or not the measurements represent an independent constraint on $^{60}Fe/^{56}Fe°_{SSI}$ remains open to debate.

Analysis of chondrules from the CB_a meteorite Gujba and ungrouped 3.05 ordinary chondrite NWA 5717 by Tang and Dauphas (2012) form near horizontal arrays that yield $^{60}Fe/^{56}Fe°$ from $1\text{-}3x10^{-9}$. However, elemental mapping by Telus et al. (2016) showed that chondrules in all chondrites they studied had experienced some open system behaviour of Fe and Ni. Only the most pristine, LL3.0 meteorite, Semarkona, retained undisturbed chondrules, about ~40% of those studied. Prompted by these findings, Tang and Dauphas (2015) made measurements of single chondrules from Semarkona, to yield a valuable but still relatively poorly defined $^{60}Fe/^{56}Fe° = (5\pm3)x10^{-9}$. The lack of significant differences between $^{60}Fe/^{56}Fe°$ for these meteorites of different metamorphic grade suggests that they are not unduly compromised by this open system behaviour. Given an average chondrule age of 2Ma post CAI (see recent compilation of data in Budde et al., 2016), the $^{60}Fe/^{56}Fe°_{SSI} \sim 9x10^{-9}$ derived from these individual chondrule measurements is notably compatible with the studies from achondrite meteorites. In a grand compilation of various determinations of $^{60}Fe/^{56}Fe°$ from bulk measurements, Tang and Dauphas (2015) derived a weighted average $^{60}Fe/^{56}Fe°_{SSI} = (1.0\pm0.3)x10^{-8}$.

In contrast to the work described above on Ni separated from bulk samples, much higher $^{60}Fe/^{56}Fe°$ have been inferred from *in situ* work by SIMS. Initially, the absence of detectable differences in the $^{60}Ni/^{61}Ni$ of olivines from type II chondrules from Semarkona, relative to terrestrial olivines, was used to place an upper limit of $3.4x10^{-7}$ on their $^{60}Fe/^{56}Fe°$ (Kita et al., 2000). However, later studies documented correlated $\varepsilon^{60}Ni$ and Fe/Ni in matrix sulfides and oxides from primitive ordinary chondrites suggesting $^{60}Fe/^{56}Fe°$ from $1x10^{-7}$ to $1x10^{-6}$ (Tachibana and Huss, 2003; Mostefaoui et al., 2004, 2005; Guan et al., 2007). As the time of formation of these phases is uncertain, the significance of these data arrays for inferring $^{60}Fe/^{56}Fe°_{SSI}$ was open to question. In an elegant study, Tachibana et al. (2006) subsequently analysed different phases from the chondrules of Semarkona. Although the ranges in correlated Fe/Ni and $\varepsilon^{60}Ni_{62/61}$ were lower than in the sulfide work, interpretation of the arrays as constraining $^{60}Fe/^{56}Fe°_{SSI}$ $(5\text{-}10)x10^{-7}$ seemed less equivocal. Similar results were reported by Mishra et al. (2010) for single chondrule analyses from a wider range of unequilibrated ordinary chondrites. Yet, all such analyses are controlled by the errors on the very small ^{61}Ni and ^{62}Ni beams used for determining $\varepsilon^{60}Ni_{62/61}$ (the larger ^{58}Ni beam cannot be used as it is interfered by ^{58}Fe). These measurements thus critically require accurate background determination and interference free spectra. Moreover, the use of the minor Ni isotope in the denominator of such low intensity measurements can lead to a statistical bias in calculated ratios (Ogliore et al., 2011, see also Coath et al., 2013). This artefact resulted spurious correlations between Fe/Ni and $\varepsilon^{60}Ni_{62/61}$ in all earlier work (Telus et al., 2012). Yet subsequent work has continued to report high inferred $^{60}Fe/^{56}Fe°$ (see Fig. 6c) from *in situ* analyses of chondrules in studies for which such statistical bias is argued to be insignificant (Mishra and Goswami, 2014; Mishra and Chaussidon, 2014; Mishra et al., 2016).

Hence, inferred $^{60}Fe/^{56}Fe°$ from TIMS/MC-ICPMS studies and SIMS analyses of individual chondrules are markedly different. This contrast in conclusions from bulk and *in situ* approaches also extends to other MC-ICPMS work. Regelous et al. (2008) and Steele et al. (2012) obtained the loose constraint that the $^{60}Fe/^{56}Fe°$ of carbonaceous chondrites was $<1x10^{-7}$, given their

indistinguishable compositions relative to IVB iron meteorites. Tang and Dauphas (2012) noted that the constant $^{58}Fe/^{54}Fe$ in all their analyses was incompatible with nucleosynthetic models that could account for $^{60}Fe/^{56}Fe°_{SSI}$ ~$1x10^{-6}$. Explicit comparison can be made between SIMS and MC-ICPMS data for individual chondrule analyses from Semarkona, reported in the studies of Mishra and Chaussidon (2014) and Tang and Dauphas (2015) respectively. The former inferred $^{60}Fe/^{56}Fe°$ $(3±2)x10^{-7}$ whereas the latter, as discussed above, argued for $(1±3)x10^{-9}$. Although a detailed comparison requires knowledge of individual chondrule ages (e.g. Mishra et al., 2010) which can be variable (see Connelly et al. 2012), this cannot account for the two orders of magnitude difference in the results of the two studies. It is also worth noting that a SIMS study of basaltic achondrites reported $^{60}Fe/^{56}Fe° = (6±9)x10^{-9}$ for quenched angrites (Siguira et al 2006), in good agreement with the MC-ICPMS studies (Quitté et al, 2010; Spivak-Birndorf, 2011; Tang and Dauphas, 2012; Tang and Dauphas, 2015). Thus the divergent results between SIMS and MC-ICPMS are seem restricted to analyses of chondrules.

The difference in inferred $^{60}Fe/^{56}Fe°_{SSI}$ between the bulk and *in situ* studies continues to be debated, see Mishra et al. (2016) and Tang and Dauphas (2015). Although we cannot offer an unbiased opinion, we argue strongly for the validity of the interpretations based on MC-ICPMS and TIMS analyses. Not only does this work show consistency in values obtained on a range of materials, from chondrules to bulk achondrites, but the approach removes sample matrix before analysis. The high Fe/Ni SIMS analyses typically collect only ~10000 counts of the minor Ni isotopes and apply a background correction determined from a single point on the mass spectrum. Perhaps most critically, the *in situ* approach has not documented accurate ^{60}Ni measurement for materials with the highest Fe/Ni, that define the isochrons (see Fig. 6c).

In this light, we note there may be a possible interference problem for SIMS analyses from the presence of $^{59}CoH^+$. Even for high resolution SIMS measurements, $^{59}CoH^+$ overlaps considerably with $^{60}Ni^+$ (Mishra and Chaussidon, 2014) and depending on measurement mass, it may not be resolved at all. The high Fe/Ni portions of chondrules are the result of fractional removal of olivine and/or low-Ca pyroxene and troilite from the cooling melt droplet. Ni is considerably more compatible than Fe in these fractionating phases and so the residual melt (and phases that subsequently crystallise from it) acquire high Fe/Ni. Ni is also more compatible than Co under the same conditions and so as crystallisation proceeds, Co/Ni will also increase. Thus high Fe/Ni in chondrules is inevitably associated with high Co/Ni. We have quantified this process in Fig 7, using the partition coefficients from experiments designed to mimic crystallisation of chondritic liquids at low pressure and which provide simultaneously determined Fe, Ni and Co data (Gaetani and Grove, 1995). In detail, the evolution of Fe/Ni and Co/Ni depend on the amount of fractionating sulfide. We examine two scenarios using relatively low (0.2%) and high (1%) amounts of sulfide for Semarkona Type II chondrules, taken from the work of Jones (1990). Although this parameter changes the amount of crystallisation required to reach a given Fe/Ni, the amount of sulfide little affects the overall trend. We show that the extreme $^{56}Fe/^{58}Ni$ ~ 7000 of the key SIMS analyses will be associated with $^{59}Co/^{60}Ni$ ~200 (Fig. 7). This is the model value for a ferro-magnesian phase (specifically olivine) grown from the residual melt, as this was the main target in the study of Mishra and Chaussidon (2014). Assuming that the fraction of hydride production determined for iron ($^{56}FeH/^{56}Fe$ ~ $5x10^{-5}$, Mishra and Chaussidon, 2014) can be used for cobalt, this implies a ^{59}CoH contribution of 1% on the mass 60 peak (i.e. $\Delta^{60}Ni$ ~10), sufficient to explain the anomalous ^{60}Ni reported. This suggested explanation of the divergence of bulk and *in situ* inferences can be tested by measuring Co intensities during SIMS analysis.

In summary we infer $^{60}Fe/^{56}Fe°_{SSI}$ ~$1x10^{-8}$, although this is not a consensus view. This conclusion implies that the solar system did not form with $^{60}Fe/^{56}Fe$ discernibly different from ISM. Thus if the elevated ^{26}Al of the solar system is to be explained by recent injection of stellar material, this must come from a source which does not also generate significant ^{60}Fe. Tang and Dauphas (2012) suggest that winds from the outer portions of a giant, Wolf-Rayet star could

constitute an appropriate explanation. These results argue against a supernova trigger of solar system collapse (see Wasserburg et al., 1998).

4. MASS-DEPENDENT Ni ISOTOPIC VARIABILITY

4.1 Magmatic Systems

Mass-dependent Ni isotopic variations in magmatic systems have received relatively little interest. This may be due to the lack of redox variability of Ni in common silicate phases on Earth, which has been a prime driver for exploration of several other isotopic systems, based on the notion that redox related changes in bonding environment will lead to large mass-dependent fractionations. However, the notable change in Ni oxidation state from 2+ to 0 and partitioning during core formation provides a significant point of interest.

In common with many other isotopic systems recently investigated, commercially available metals can show marked mass-dependent isotopic variability. For example, Tanizuma and Hirata (2006) reported a range of 0.6‰ in the $\delta^{60/58}$Ni of a selection of high purity commercial Ni reagents. The authors noted the potential of isotopic fractionation during purification of Ni by the Mond process, which involves separation of Ni in the vapour phase as the volatile $Ni(CO)_4$ species. However, two Ni ores analysed by Tanziuma and Hirata (2006) showed an even greater variability ($\delta^{60/58}$Ni = 0.5 to -0.4), spanning the compositions of the laboratory Ni reagents and making it hard to distinguish the influences of anthropogenic from natural fractionation. An important consequence of the fractionated values of $\delta^{60/58}$Ni seen in purified Ni is that NBS SRM 986 is sadly not representative of bulk terrestrial reservoirs, either in mass-dependent (Cameron et al., 2009; Steele et al., 2011; Gall et al., 2012; Gueguen et al., 2013) or mass-independent Ni isotopic compositions (Steele et al., 2011). The latter likely stems from imperfect mass-bias correction using a single exponential form for combined instrumental, natural and industrial fractionations. Separation of Ni as a carbonyl species in the Mond process but its measurement as an elemental ion in mass spectrometry offers a tangible mechanism to account for this feature (Steele et al., 2011). Although cosmetically unappealing, the slight deviation of the Ni reference standard from bulk terrestrial values does not dimish its value as a common datum.

As a planetary reference Moynier et al. (2007) reported $\overline{\delta}$Ni for a wide range of iron meteorites and metal phases in chondrites. Planetary cores dominate the Ni budgets of planets and planetesimals, so iron meteorites should provide a representative mass-dependent Ni isotopic composition of their parent body. Likewise a metal phase will control the Ni bulk composition of host chondrites. These sample-standard bracketing data of Moynier et al. (2007) are replotted as $\delta^{60/58}$Ni in Fig. 8a and vary from 0-0.8‰ with an average ~0.3 ‰ (individual errors ~±0.15‰). Cameron et al. (2009) presented $\delta^{60/58}$Ni for a representative selection of bulk chondrite and iron meteorites by double spiking, which showed less scatter than the Moynier et al (2007) data but with a similar average of 0.27±0.06 ‰. A set of iron meteorites measured by sample-standard bracketing (Chernonozhkin et al., 2016) and two higher precision double-spiked measurements of chondrites Steele et al. (2012) fall within this range. These studies are combined to give a planetary reference of $\delta^{60/58}$Ni = 0.24±0.04 (Table 2). Whilst there may be systematic differences in $\delta^{60/58}$Ni between different meteorite types (cf. Luck et al., 2003), given the limited number of samples currently available and their small variability relative to precision, we have done no more than to compile this average, which implicitly assumes a uniform bulk Ni mass-dependent isotopic composition for different planetary objects in the solar system.

To date, most literature $\delta^{60/58}$Ni analyses of peridotitic material or mantle derived melts, appropriate for estimating the composition of the silicate Earth, are reference materials. In their assessment of a baseline value for silicates, Cameron et al. (2009) found that samples from peridotite to granite, in addition to a range of continental sediments varied little, $\delta^{60/58}$Ni =0.15±0.24. Combining two higher precision measurements of fresh peridotites with the data of

595 Cameron et al. (2009), Steele et al. (2011) calculated a weighted average of 0.18±0.04 ‰ for the silicate Earth. Additional analyses of mafic and ultra-mafic samples by Gall et al. (2012), Gueguen et al. (2013) and Chernonozhkin et al. (2015) support such isotopically lighter values of the terrestrial mantle relative to the meteorite reference (Fig. 8). Gueguen et al. (2013) compiled analyses of silicate samples to calculate $\delta^{60/58}$Ni = 0.05±0.05 for bulk silicate Earth. The latter
600 includes measurements of deep sea clays, as representative of the continental crust. Given the likely pelagic component of some Ni in these sediments and possible associated isotopic fractionations (see below), coupled with the trivial contribution of crustal Ni to bulk silicate Earth, the inclusion of these sediments is unwarranted but does not unduly bias the estimate. Revising this value to include only samples of the mantle and mantle derived melts, a better
605 defined $\delta^{60/58}$Ni = 0.11±0.04 is obtained for the bulk silicate Earth (Table 2).

These data thus imply that the bulk silicate Earth is slightly isotopically light relative to a bulk planetary reference, by ~0.15 ‰. Most plausibly this is the result of core formation, as Ni is a siderophile element and strongly partitioned into the metal phase. The sense of isotopic
610 fractionation between the silicate Earth and chondrites is consistent with the isotope partitioning experiments of Lazar et al. (2012), who determined a fractionation factor between metal and talc, $\Delta^{62/58}Ni_{metal\text{-}silicate} = (0.25\pm0.02)x10^6/T^2$. Using this expression to calculate isotopic fractionation between metal and silicate during core formation predicts a rather more modest than observed difference between bulk and silicate Earth of ~0.02 ‰ for a single core-mantle equilibrium at
615 2500 K. Yet, as the authors note, larger net fractionations are possible for a Rayleigh process with a well mixed mantle magma ocean. Clearly, there is also scope for measuring isotopic fractionation under conditions that more closely approximate core formation, although these are difficult experiments. Empirical constraints on high temperature fractionation factors could potentially be gleaned from the analyses of some metal and silicate separates from mesosiderites
620 and pallasites presented by Chernonozhkin et al. (2016). However, the sense of fractionation between metal and silicate in the two meteorite types is inconsistent and an important role for kinetic (diffusive) fractionation during cooling seems likely (Chernonozhkin et al., 2016).

In contrast to the relative constancy of $\delta^{60/58}$Ni in many silicate samples noted above, Steele
625 et al. (2011), Gueguen et al. (2013) and Hofmann et al. (2014) reported a wide range of isotopically light values ($\delta^{60/58}$Ni = -0.1 to -1) in Ni-bearing sulfides from komatiitic magmas, see Fig. 8b. Such ores are believed to be formed by sulfide saturation following crustal assimilation by these ultra-mafic magmas (Huppert et al., 1984). The Ni in the sulfides is dominantly from the mantle derived melts and so the data imply a significant Ni isotopic fractionation between
630 sulfide and silicate magma, although kinetic effects may also play a role. These low $\delta^{60/58}$Ni echo the value of -0.34‰ measured previously for a millerite ore from the Thompson Ni Belt (Manitoba, Canada) by Taminura and Hirata (2006). Despite experiencing some secondary reworking, these Ni deposits were similarly formed by the interaction of ultra-mafic melts with crustal sulfides (e.g. Bleeker and Macek, 1996) and so this process generally seems to result in
635 low $\delta^{60/58}$Ni. On the other hand, an isotopically heavy pentlandite from Sudbury ($\delta^{60/58}$Ni ~0.5) was reported by Taminura and Hirata (2006). These sulfides were formed from a meteorite impact induced melt sheet, with the Ni largely sourced from the molten continental crust (Walker et al., 1991). This different source of Ni for the Sudbury ore relative to the komatiite hosted samples is a plausible explanation of their contrasting $\delta^{60/58}$Ni. Another style of Ni ore deposit,
640 produced from lateritic weathering of ultramafic lithologies in Brazil, exhibits less anomalous compositions, $\delta^{60/58}$Ni = 0.02-0.2 (Ratié et al., 2016), implying little net fractionation during their formation.

4.2 Ni isotope fractionation during weathering and the hydrological cycle.

645 As discussed above, there is currently only a single experiment to underpin understanding of the controls on Ni isotopic fractionation at magmatic temperatures (Lazar et al., 2012). In contrast, isotopic fractionations between Ni species relevant for the hydrological cycle have received more extensive, theoretical investigation (Fujii et al. 2011; Fujii et al. 2014). Despite

the absence of redox changes at the Earth's surface, differences in the bonding environment between common, aqueous Ni species result in significant isotopic fractionations (Fig. 9). These first principles calculations for a homogenous aqueous system provide a useful guide to potential magnitudes of Ni isotopic fractionation but do not currently provide direct information on the effects of sorption of Ni onto Fe/Mn oxide surfaces, for example, which likely play an important role in the surface cycle of Ni (e.g. Peacock and Sherman, 2007). However, experimental work by Wasylenki et al. (2015) documents that sorption of Ni onto the ferrihydride favours the lighter isotopes, leaving an isotopically heavier residual Ni in solution (Fig. 9).

The processes of weathering, transport to and removal from the ocean can result in major isotopic fractionations, such that the isotopic composition of seawater is a notable end-member for a number of elements (e.g. Li, B, Mg, Mo). In a comprehensive study of seawater, the first to define its Ni isotopic composition, Cameron and Vance (2014) reported $\delta^{60/58}$Ni =1.44±0.15 which is near constant across all ocean basins and at various depths. Seawater is thus markedly isotopically heavy relative to typical silicate rocks (Fig. 8b,c). Cameron and Vance (2014) further documented that the dissolved Ni loads of rivers are dominantly isotopically heavy relative to unaltered silicates (Fig. 8b,c), showing that weathering processes result in significant Ni isotopic fractionation. Similarly, the $\delta^{60/58}$Ni ~0.5 of organic-rich marine shales (Fig. 8d) is argued to reflect the end product of the weathering process (Porter et al., 2014), as is also likely the case for the more modestly elevated $\delta^{60/58}$Ni of coal and banded ironstone formation (BIF) standards (Gueguen et al., 2013). As a corollary, several studies have shown that soils (Fig. 8d), the residues of weathering, are commensurately isotopically light (Estrade et al., 2015, Ratié et al. 2014, Gall et al., 2013).

A major sink of Ni in the oceans is its incorporation into Fe-Mn crusts (e.g. Peacock and Sherman, 2007). A detailed study of these materials by Gall et al. (2013) showed $\delta^{60/58}$Ni that ranged from 0.9-2.5 ‰, with modern samples yielding an average of 1.6±0.8 ‰ (Fig. 8c). This work found little systematic variation in the $\delta^{60/58}$Ni of samples between ocean basins or indeed over an ~80 Ma record in the Pacific. In large part, it appears that the $\delta^{60/58}$Ni of Fe-Mn crusts reflects the isotopically heavy composition of seawater and so this sink does not represent a major source of isotopic fractionation as is the case in the Mo isotope cycle (e.g. Barling et al. , 2001). Earlier in geological history, sorption of Ni to iron oxide phases, preserved in BIF, may have been a significant sink for oceanic Ni. The near constant $\Delta^{60/58}Ni_{dissolved\text{-}sorbed}$ = 0.35±0.10 determined by for Ni sorption onto ferrohydrite over a range of conditions (Wasylenki et al., 2015) gives encouragement for recovering information on past ocean compositions from BIF. It is worth noting that this fractionation, however, is in the wrong direction to account for the isotopic difference between seawater and modern Fe-Mn crusts (Fig. 8c) by such a sorption process. On the other hand, the sense of fractionation could help account for the isotopically heavy composition of Ni in rivers as the product of weathering.

Although the first order observations on the hydrological cycling of Ni isotopes have thus recently been outlined, the isotopic balance of Ni is still not obviously complete (Cameron and Vance, 2014) and this further echoes a long identified elemental imbalance between oceanic inputs and outputs for Ni (e.g. Krishmaswami, 1976). Whilst rivers are isotopically heavy inputs to the oceans, the oceans are ~0.6 ‰ heavier than the mean riverine input. There always remains an uncertainty over the representativeness of the river sample, but the magnitude of the Ni isotopic mis-match is troublesome. Since Fe-Mn crusts are isotopically heavier, on average, they do not provide a ready explanation to the problem. A tempting scenario would be to invoke the role of kinetic isotopic fractionation of Ni resulting from its essential role in several biological pathways in the marine environment (see below). Yet the lack of difference in $\delta^{60/58}$Ni between surface and deep water limits the magnitude of this light isotope sink (Cameron and Vance, 2014). Potential solutions to resolve this imbalance are discussed by Cameron and Vance (2014) who tentatively propose the release of Ni carried on Fe-Mn coatings from the suspended load during esturine processes. The authors argue against the role of serpentinisation, given an

absence of vertical $\delta^{60/58}$Ni variation in the water column. Yet, a single, oceanic serpentine sample reported by Gueguen et al. (2013) is notably isotopically light ($\delta^{60/58}$Ni = -0.13), at high [Ni] ~1500ppm and so tantalisingly hints at a plausible reservoir to complement the isotopically heavy oceans.

Most recently, however, measurements of isotopically heavy Ni ($\delta^{60/58}$Ni ~2) in euxinic deep waters of the Black Sea (Vance et al., in review) appear to be the complement to partial removal to the sediment pile of a sorped, Ni sulfide species, which Fujii et al. (2011) predicted to be isotopically light (Fig. 9). If such a process occurred more generally in the sediment interface on upwelling margins of the Pacific, which become euxinic a few centimetres below the surface, this might provide an answer to oceanic Ni isotopic balance (Vance et al., in review).

4.3 Biological Mass-dependent Fractionations

As with some other first row transition elements, Ni plays an important role in several biogeochemical cycles. It is an essential trace element for key enzymes in methane production and decomposition of urea. Kinetic fractionation in metabolic pathways will favour the least strongly bound, lightest isotopes and given this basic notion it might be anticipated that Ni incorporated into biological systems would have low $\delta^{60/58}$Ni. On the other hand, the first principles calculations (Fujii et al., 2011; Fujii et al., 2014) show substantial equilibrium fractionation of Ni isotopes between aqueous species complexed with different naturally occurring organic ligands (Fig. 9). Fractionation factors at 298K, calculated between the hexa-aqua ion, the dominant Ni species over a range of conditions in natural waters and complexes with oxalate, phosphate and citrate ions are shown in Figure 9. These examples are indicative of the range of fractionations reported by Fujii and co-workers. Moreover they serve as model representations of possible bonding environments for Ni in soils and plants (Fujii et al., 2011; Fujii et al., 2014). If biological pathways efficiently discriminate between such species, macroscopic Ni isotopic variability can result. Yet, some caution needs to be exercised in using simple equilibria to predict the effects of a complex biochemical reaction sequence. For example, the inorganic oxidation of iron results in a 2.75‰ ^{56}Fe/^{54}Fe isotopic fractionation at room temperature (Johnson et al., 2002), whereas if this processes is biologically mediated through iron oxidising bacteria, a much smaller 1.5‰ fractionation is observed (Croal et al., 2004).

Given the critical role of Ni in biological methanogenesis, it might be anticipated that Ni isotopic fractionation would be associated with species that had evolved to incorporate environmental Ni to these ends. In a reduced environment, such as the early Earth, methanogens likely represent a major component of the surface Ni cycle and have the potential to impart an isotopic record of their presence. In the first study to look at the effects of biological processes on Ni isotope compositions, Cameron et al. (2009) examined Ni isotopic fractionations during laboratory growth of 3 species of methanogens (2 mesophiles, *Methanosarcina barkeri* and *Methanosarcina acetivorans* and one hyperthermophile, *Methanococcus jannaschii*) and one non-methanogen, a heterotrophic archea (*P. calidifontis*) as reference. Cameron et al. (2009) showed that Ni incorporated into all three methanogens was isotopically light compared to the media in which they grew, $\Delta^{60/58}Ni_{cells\text{-}media}$ ~ -1 but $\Delta^{60/58}Ni_{cells\text{-}media}$ ~0 for the heterotrophic archea, *P.Calidifontis* (Fig. 9).

These substantial fractionations show promise as a means for identifying the active role of methanogens in the rock record of the early Earth. As noted earlier, there is a near constant and smaller fractionation when Ni is sorbed from aqueous solution to ferrihydrite (Wasylenki et al., 2015) and further experiments suggest that such Ni remains immobile during subsequent diagnesis (Robbins et al., 2015). Hence the isotopic composition of Ni in BIF, originally sorbed from Archaen seawater is anticipated to be isotopically heavy for a system in which methanogens dominated the marine Ni cycle. Analyses of BIF of different ages therefore should provide a possible means to investigate the proposed demise of the methanogens prior to the rise in

atmospheric oxygen ~2.4 Ga (Konhauser et al., 2009). Yet other fractionations could possibly produce a similar signature (Fig. 7). As discussed above, the partial removal of an isotopically light Ni sulfide species has been invoked to account for modern ocean Ni mass balance. This process can impart a similar sense and magnitude of Ni isotopic fractionation to residual ocean water as Ni sequestration by methanogens (Fig. 9). Such *partial* removal of sulfide species, however, seems unlikely to have occurred under the fully reduced oceanic conditions of the Archean and should have become more important at the onset of oxidation- the converse to that expected from the activity of methanogens.

Ni is an essential micro-nutrient in higher plants (e.g. Brown et al. 1987) given its functional presence in the enzyme urease (Dixon et al., 1975). However, Ni abundances as low as 90ng/g can be sufficient to maintain this function (Dixon et al., 1975) and so plants do not represent a large Ni reservoir, with Ni concentrations typically less than 10µg/g. Exceptions are the so-called Ni hyperaccumulators, that have evolved to be tolerant of Ni rich soils that develop on ultramafic lithologies. Many plants deal with the toxicity of metals by sequestering them in their roots, but hyperaccumulators transport large quantities of metals to their leaves. Such Ni hyperaccumulators make interesting subjects for Ni isotopic investigation, as high Ni concentrations make them amenable to analysis and their specialisation to cope with high Ni concentrations might lead to characteristic isotopic fractionations.

Laboratory experiments (Deng et al., 2014) and a field study (Estrade et al. 2015) reported isotopic analyses for several Ni hyperaccumulators, together with a non-accumulator species for comparison. In all but one case, the plants have net isotopically light compositions relative to dissolved Ni in growth media or inferred for soil water ($\Delta^{60/58}Ni_{\text{bulk plant-solution}}$ = -0.06 to -0.8), see Figure 9. In the case of field study, fractionation factors were derived relative to the bio-available Ni obtained by extraction from the soil with diethylenetrainminepentaacetic acid (Estrade et al., 2015) and this process adds some uncertainty to the values derived. However, the isotopically heavy composition of this extractable Ni would be be consistent with predictions if $Ni(C_2O_4)_3^{2-}$ is used as a proxy for Ni bound to humic acid, as suggested by Fujii et al. (2011), and removed from the bio-available pool. The largest Ni isotopic fractionations are observed in some laboratory experiments with Ni-hyperaccumulators but in general there is not a clear distinction between hyperaccumulators and non-hyperaccumulators (Fig. 9). The overall light isotopic composition of the plants is likely the result of kinetic fractionation during Ni up-take by 'low affinity' transport systems across the cell membranes of plant roots. The dominant role of such ion channels, as opposed to 'high affinity' carried-mediated transport, had previously been invoked by Weiss et al. (2005) to account for the light bulk Zn isotopic compositions of plants they studied.

Isotopically lighter Zn in shoots relative to roots was first reported by Weiss et al., (2005) and similar features are observed in the Ni isotopic studies of plants (Deng et al., 2014; Estrade et al., 2015). In a comparison of shoot-root isotopic differences of Zn and Ni in the same species, Deng et al. (2014) noted a more modest fractionations for Ni. They attributed this to higher Ni mobility in plants relative to Zn. It should be re-emphasised that most of the species analysed for their Ni isotopic compositions are hyperaccumulators, in which Ni is anomalously enriched shoots relative to roots. The two non-accumulators studied so far show contrasting behaviour, with both positive, *Thlapsi arvensa* (Deng et al., 2014) and negative, *Euphorbia spinosa* (Estrade et al., 2015) values of $\Delta^{60/58}Ni_{\text{shoots-roots}}$, see Figure 9. Some variability in $\Delta^{60/58}Ni$ between roots, stems and leaves may be related to the growth stage of the plants (Estrade et al., 2015). A full explanation of the diverse results requires more detailed work on the transport of Ni in plants, which is currently poorly understood. However, these data do provide a means to assess the generality of a hypothesis proposed to explain plant isotopic variability Zn system. Fujii and Albarède (2012) invoked isotopic fractionations between Zn phosphate species concentrated in the roots and citrates and malates in the leaves. In the case of Ni, however, Fujii et al. (2014) calculated that no discernible fractionations are predicted for this mechanism (Fig. 9) and so this cannot explain the root-shoot variability in $\delta^{60/58}Ni$.

Not only is Ni incorporated by living plants, but also during diagenesis of plant matter Ni frequently becomes bound by porphyrins, derived from chlorophyll, that originally complexed Mg. As an important trace element in oils, the abundance of Ni has, especially in relation to V, long been used as a tracer of source and evolution of oil reservoirs (e.g. Hodgson, 1954). Adding the additional constraint of the Ni isotopic composition of crude oils is an intriguing new means to understand oil formation. A preliminary study by Ventura et al. (2015) report $\delta^{60/58}$Ni (together with V and Mo isotopic compositions) for a global selection of crude oils. These show a limited range of $\delta^{60/58}$Ni from 0.4 to 0.7, which overlaps the composition of organic-rich shales (Fig. 8c).

5. OUTLOOK

There are exciting prospects for Ni isotopic measurements across the fields outlined above.

Although the most anomalous macroscopic objects in the solar system, CAIs have not been systematically studied for their Ni isotopic compositions and rather few analyses currently exist. A recent study has reported extreme $\varepsilon^{64}Ni_{61/58}$ (up to 55) in two Allende CAIs (Chen and Papanastassiou, 2014). Further investigation of Ni isotopic compositions of CAIs and their relation to anomalies of other neutron rich nuclides would be valuable (e.g. recent discussion by Chen et al., 2015). More generally, finding the carrier that is responsible for bulk meteoritic Ni isotopic variation is a key quest.

It is clearly critical to resolve definitively the value of $^{60}Fe/^{56}Fe°_{SSI}$, given its implications for the seeding of the solar system with exotic isotopic signatures. We strongly favour low values of $^{60}Fe/^{56}Fe°_{SSI}$, consistent with background ISM, but a community consensus is required. We suggest that exploring the potential role of interfering CoH^+ as highlighted in section 3 would be a useful step forward.

The measurable abundances of Ni in both silicate and iron meteorites allows valuable comparison of different meteoritic objects. To date this has shown that in contrast to the other magmatic irons so far analysed, the IVB iron meteorites have affinities with carbonaceous rather than ordinary chondrites. It would be useful to make a more comprehensive investigation of these genetic relationship in other, so far unanalaysed meteorite types.

As with Mg, for which Ni typically substitutes, there appears to be little mass-dependent Ni isotopic fractionation during silicate partial melting and differentiation. This observation would benefit from more detailed study and unpublished work by Gall (2011) suggests that there might be some systematic silicate melt-solid fractionations at magmatic temperatures. Publication of these and additional empirical data in conjunction with experimental determinations of fractionation factors would be helpful. In the absence of major fractionations during silicate differentiation, the small, but apparently significant fractionation of Ni isotopes during core formation becomes of interest, but a more robust estimate of bulk silicate Earth is required. The current value relies heavily on a few reference standards. Additional observations of $\delta^{60/58}$Ni on the silicate mantles of smaller planetary bodies, where the effect might be larger (due to greater Ni partitioning into the core at low pressure), should prove informative. Interpretation of such results would greatly benefit from further experimental determinations of silicate-metal fractionation factors.

Better understanding the seemingly significant fractionation of Ni isotopes during weathering processes and a clear resolution of the apparent isotope imbalance in the ocean are obvious targets for future research. Comparisons with the better studied, non-redox sensitive, divalent cations, Mg and Ca, would be welcome. The contrast in oceanic sinks for these different

elements (Fe-Mn crusts, versus seafloor alteration versus carbonate production) makes differences in their behaviour through time of considerable interest.

As with other novel, isotopic systems, their nascent application to biological systems carries unknown potential. The large Ni isotopic fractionation of methanogens is a specifically appealing prospect, but whether or not such Ni isotopic fractionations remains locked in the rock record and sufficiently distinct over background variability, including abiotic reactions in the weathering environment, remains to be seen.

ACKNOWLEDGEMENTS

In the writing of this review TE was supported by the ERC (AdG 321209 ISONEB) and RCJS by ETH. This funding is gratefully acknowledged. The authors wish to thank the Editor for his patience and two anonymous reviewers for numerous useful suggestions, kindly pointing to some egregiously missed references and encouragement to expand the final section to speculate in a field in which we have limited expertise. A timely, final sanity check by Derek Vance and access to his unpublished manuscript was appreciated. The authors would like to doff their caps to the many who have helped in the development of their ideas about the Ni system, not least Chris Coath, Marcel Regelous, Hart Chen, Matthias Willbold, Derek Vance, Vyll Cameron and Corey Archer,

REFERENCES

Albalat, E., P. Telouk, and F. Albarède, Er and Yb isotope fractionation in planetary materials. (2012) *Earth Planet. Sci. Lett.* **355-356**, p. 39-50.

Amelin, Y., A.N. Krot, I.D. Hutcheon, and A.A. Ulyanov, Lead isotopic ages of chondrules and calcium-aluminum-rich inclusions. (2002) *Science* **297**, p. 1678-1683.

Amelin, Y., U-Pb ages of angrites. (2008a) *Geochim. Cosmochim. Acta* **72**, p. 221-232.

Amelin, Y., The U-Pb systematics of angrite Sahara 99555. (2008b) *Geochim. Cosmochim. Acta* **72**, p. 4874-4885.

Barling, J., G.L. Arnold, and A.D. Anbar, Natural mass-dependent variations in the isotopic composition of molybdenum. (2001) *Earth Planet. Sci. Lett.* **193**, p. 447-457.

Birck, J.-L. and C.J. Allègre, Evidence for the presence of ^{53}Mn in the early solar system. (1985) *Geophys. Res. Lett.* **12**, p. 745-748.

Birck, J.L. and G.W. Lugmair, Nickel and chromium isotopes in Allende inclusions. (1988) *Earth Planet. Sci. Lett.* **90**, p. 131-143.

Bizzarro, M., J.A. Baker, H. Haack, and K.L. Lundgaard, Rapid timesclaes for accretion and melting of differentiated planetesimals inferred from ^{26}Al-^{26}Mg chronometry. (2005) *Astrophys. J.* **632**, L41-L44.

Bizzarro, M., D. Ulfbeck, A. Trinquier, K. Thrane, J.N. Connelly, and B.S. Meyer, Evidence for a late supernova injection of Fe-60 into the protoplanetary disk. (2007) *Science* **316**, p. 1178-1181.

Bizzarro, M., D. Ulfbeck, J.A. Boyd, and H. Haack, Nickel isotope anomalies in iron meteorites. (2010) *Meteorit. Planet. Sci.* **45**, A15.

Blichert-Toft, J., F. Moynier, C.-T.A. Lee, P. Telouk, and F. Albarède, The early formation of the IVA iron meteorite parent body. (2010) *Earth Planet. Sci. Lett.* **296**, p. 469-480.

Bleeker, W. and J.J. Macek, 1996. Evolution of the Thompson Nickel Belt, Manitoba: setting of Ni-Cu deposits in the western part of the circum superior boundary zone; Fieldtrip Guidebook Geological Association of Canada Annual Meeting, Winnipeg, Manitoba.

Brennecka, G.A. and M. Wadhwa, Uranium isotope compositions of the basaltic angrite meteorites and the chronological implications for the early Solar System. (2012) *Proc. Natl. Acad. Sci. USA.* **109**, p. 9299-9303.

Brown, P.H., R.M. Welch, and E.E. Cary, Nickel: a micronutrient essential for higher plants. (1987) *Plant Physiol.* **85**, p. 801-803.

Budde, G., T. Kleine, T.S. Kruijer, C. Burkhardt, and K. Metzler, Tungsten isotopic constraints on the age and origin of chondrules. (2016) *Proc. Natl. Acad. Sci. USA* **113**, p. 2886-2891.

Burbidge, E.M., G.R. Burbidge, W.A. Fowler, and F. Hoyle, Synthesis of the Elements in Stars. (1957) *Rev. Mod. Phys.* **29**, p. 547-650.

Cameron, V., D. Vance, C. Archer, and C.H. House, A biomarker based on the stable isotopes of nickel. (2009) *Proc. Natl. Acad. Sci.* **106**, p. 10944-10948.

Cameron, V. and D. Vance, Heavy nickel isotope compositions in rivers and the oceans. (2014) *Geochim. Cosmochim. Acta* **128**, p. 195-211.

Chen, J.H., D.A. Papanastassiou, and G.J. Wasserburg, A search for nickel isotopic anomalies in iron meteorites and chondrites. (2009) *Geochim. Cosmochim. Acta* **73**, p. 1461-1471.

Chen, J.H. and D.A. Papanastassiou, Endemic ^{64}Ni effects in Allende Ca-Al-rich inclusions. (2014) *Lunar Planet. Sci.* **45**, p. 2327.

Chen, H.-W., T. Lee, D.-C. Lee, and L.-C. Chen, Correlation of ^{48}Ca, ^{50}Ti and ^{138}La heterogeneity in the Allende refractory inclusions. (2015) *Astrophys. J. Lett.* **806**, L21.

Chernonozhkin, S.M., S. Goderis, L. Lobo, P. Claeys, and F. Vanhaecke, Development of an isolation procedure and MC-ICP-MS measurement protocol for the study of stable isotope ratio variations of nickel. (2015) *J. Anal. Atom. Spectrom.* **30**, p. 1518-1530.

Chernonozhkin, S.M., S. Goderis, M. Costas-Rodríguez, P. Claeys, and F. Vanhaecke, Effect of parent body evolution on equilibrium and kinetic isotope fractionation: a combined Ni and Fe isotope study of iron and stony-iron meteorites. (2016) *Geochim. Cosmochim. Acta* **186**, p. 168-188.

Clayton, D.D. and L. Jin, A new interpretation of ^{26}Al in meteoritic inclusions. (1995) *Astrophys. J.* **451**, p. L87-L91.

Clayton, R.N., L. Grossman, and T.K. Mayeda, A component of primitive nuclear composition in carbonaceous meteorites. (1973) *Science* **182**, p. 485-488.

Clayton, R.N., T.K. Mayeda, E.J. Olsen, and M. Prinz, Oxygen isotope relationships in iron meteorites. (1986) *Earth Planet. Sci. Lett.* **65**, p. 229-232.

Coath, C.D., R.C.J. Steele, and W.F. Lunnon, Statistical bias in isotope ratios. (2013) *J. Anal. Atom. Spectrom.* **28**, p. 52-58.

Cochran, W.G., Sampling Techniques. New York, Wiley and Sons (1977).

Connelly, J.N., M. Bizzarro, K. Thrane, and J.A. Baker, The Pb-Pb age of angrite SAH99555 revisited. (2008) **72**, p. 4813-4824.

Connelly, J.N., M. Bizzarro, A.N. Krot, A. Nordlund, D. Wielandt, and M.A. Ivanova, The absolute chronology and thermal processing of solids in the protoplanetary disk. (2012) *Science* **338**, p. 651-655.

Cook, D.L., M. Wadhwa, P.E. Janney, N. Dauphas, R.N. Clayton, and A.M. Davis, High precision measurements of non-mass-dependent effects in nickel isotopes in meteoritic metal via multicollector ICPMS. (2006) *Anal. Chem.* **78**, p. 8477-8484.

Cook, D.L., R.N. Clayton, M. Wadhwa, P.E. Janney, and A.M. Davis, Nickel isotopic anomalies in troilite from iron meteorites. (2008) *Geophys. Res.Lett.* **35**, L01203.

Dauphas, N., D.L. Cook, A. Sacarabany, C. Frohlich, A.M. Davis, M. Wadhwa, A. Pourmand, T. Rauscher, and R. Gallino, Iron 60 evidence for early injection and efficient mixing of stellar debris in the protosolar nebula. (2008) *Astrophys. J.* **686**, p. 560-569.

Dauphas, N., L. Remusat, J.H. Chen, M. Roskosz, D.A. Papanastassiou, J. Stodolna, Y. Guan, C. Ma, and J.M. Eiler, Neutron-rich chromium isotope anomalies in supernova nanoparticles. (2010) *Astrophys. J.* **720**, p. 1577-1591.

Deng, T.-H.-B., C. Cloquet, Y.-T. Tang, T. Sterckeman, G. Echevarria, N. Estrade, J.-L. Morel, and R.-L. Qiu, (2014) *Environ. Sci. Technol.* **48**, p. 11926-11933.

Dixon, N.E., C. Gazzola, R.L. Blakeley, and B. Zerner, Jack bean urease (EC 3.5.1.5). Metalloenzyme. Simple biological role for nickel. (1975) *J. Am. Chem. Soc.* **97**, p. 4131-4133.

Estrade, N., C. Cloquet, G. Echevarria, T. Sterckeman, T. Deng, Y. Tang, and J.-L. Morel, Weathering and vegetation controls on nickel isotope fractionation in surface ultramafic environments (Albania). (2015) *Earth Planet. Sci. Lett.* **423**, p. 24-35.

Fujii, T., F. Moynier, N. Dauphas, and M. Abe, Theoretical and experimental investigation of nickel isotopic fractionation in species relevant to modern and ancient oceans. (2011) *Geochim. Cosmochim. Acta* **75**, p. 469-482.

Fujii, T. and F. Albarède, An initio calcuation of the Zn isotope effect in phosphates, citrates and malates and applications to plants and soils. (2012) *PLoS One* **7**, e30726.

Fujii, T., F. Moynier, J. Blichert-Toft, and F. Albarède, Density functional theory estimation of isotope fractionation of Fe, Ni, Cu and Zn among species relevant to geochemical and biological environments. (2014) *Geochim. Cosmochim. Acta* **140**, p. 553-576.

Gaetani, G.A. and T.L. Grove, Partitioning of moderately siderophile elements among olivine, silicate melt and sulfide melt: constraints on core formation in the Earth and Mars. (1997) *Geochim. Cosmochim. Acta* **61**, p. 1829-1846.

Gall, L., Development and application of nickel stable isotopes as a new geochemical tracers, (2011) PhD, Univesity of Oxford.

Gall, L., H. Williams, C. Siebert, and A.N. Halliday, Determination of mass-dependent variations in nickel isotope compositions using double spiking and MC-ICPMS. (2012) *J. Anal. At. Spectrom.* **27**, p. 137-145.

Gall, L., H.M. Williams, C. Siebert, A.N. Halliday, R.J. Herrington, and J.R. Hein, Nickel isotopic compositions of ferromanganese crusts and the constancy of deep ocean inputs and continetnal weathering effects over the Cenozoic. (2013) *Earth Planet. Sci. Lett.* **375**, p. 148-155.

Gramlich, J.W., L.A. Machlan, I.L. Barnes, and P.J. Paulsen, Absolute isotopic abundance ratios and atomic weight of a reference sample of nickel. (1989) *J. Res. NIST* **94**, p. 347-356.

Gatz, D. F., and L. Smith, L., The standard error of a weighted mean concentration—i. bootstrapping vs other methods. (1995) *Atmos. Environ*. **29**, p. 1185–1193.

Guan, Y., G.R. Huss, and L.A. Leshin, ^{60}Fe-^{60}Ni and ^{53}Mn-^{53}Cr isotopic systems in sulfides from unequilibrated enstatite chondrites. (2007) *Geochim. Cosmochim. Acta* **71**, p. 4082-4091.

Gueguen, B., O. Rouxel, E. Ponzevra, A. Bekker, and Y. Fouquet, Nickel isotope variations in terrestrial silicate rocks and geological reference materials measured by MC-ICP-MS. (2013) *Geostand. Geoanal. Res.* **37**, p. 297-317.

Gurland, J., and R.C.Tripathi, A simple approximation for unbiased estimation of the standard deviation. (1971) *Am. Stat.* **25**, p. 30–32.

Heydegger, H.R., J.J. Foster, and W. Compston, Evidence of a new isotopic anomaly from titanium isotopic ratios in meteoritic materials. (1979) *Nature* **278**, p. 704-707.

Hofmann, A., A. Bekker, P. Dirks, B. Gueguen, D. Rumble, and O.J. Rouxel, Comparing orthomagmatic and hydrothermal mineralization models for komatiite-hosted nickel desposits in Zimbabwe using multiple-sulfur, iron and nickel isotope data. (2014) *Miner. Deposita* **49**, p. 75-100.

Hodgson, G.W., Vanadium, nickel and porphyrins in crude oils of Western Canada. (1954) *Am. Assoc. Petrol. Geol. Bull.* **41**, p. 2413-2426.

Huppert, H.E., R.S.J. Sparks, J.S. Turner, and N.T. Arndt, Emplacement and cooling of komatiite lavas. (1984) *Nature* **309**, p. 19-22.

Johnson, C.M., J.L. Skulan, B.L. Beard, H. Sun, K.H. Nealson, and P.S. Braterman, Isotopic fractionation between Fe(III) and Fe(II) in aqueous solutions. (2002) *Earth Planet. Sci. Lett.* **195**, p. 141-153.

Jones, R.H., Petrology and mineralogy of Type II, FeO-rich chondrules in Semarkona (LL3.0): origin by closed-system fractional crystallisation, with evidence for supercooling. (1990) *Geochim. Cosmochim. Acta* **54**, p. 1785-1802.

Jungck, M.H.A., T. Shimamura, and G.W. Lugmair, Ca Isotope Variations in Allende. (1984) *Geochim. Cosmochim. Acta* **48**, p. 2651-2658.

Kita, N.T., H. Nagahara, S. Togashi, and Y. Morshita, A short duration of chondrule formation in the solar nebula: evidence from ^{26}Al in Semarkona ferromagnesian chondrules. (2000) *Geochim. Cosmochim. Acta* **64**, p. 3913-3922.

Konhauser, K.O., E. Pecoits, S.V. Lalonde, D. Papineau, E.G. Nisbet, M.E. Barley, N.T. Arndt, K. Zahnle, and B.S. Kamber, Oceanic nickel depletion and a methanogen famine before the Great Oxidation Event. (2009) *Nature* **458**, p. 750-753.

Krishnaswami, S., Authigenic transition elements in Pacific pelagic clays. (1976) *Geochim. Cosmochim. Acta* **40**, p. 425-434.

Kruijer, T.S., T. Kleine, M. Fischer-Gödde, C. Burkhardt, and R. Wieler, Nucleosynthetic W isotope anomalies and the Hf-W chronometry of Ca-Al-rich inclusions. (2014) *Earth Planet. Sci. Lett.* **403**, p. 317-327.

Kutschera, W., P.J. Billquist, D. Frekers, W. Henning, K.J. Jensen, M. Xiueng, R. Pardo, M. Paul, K.E. Rehm, R.K. Smither, and J.L. Yntema, Half-life of ^{60}Fe. (1984) *Nucl. Instrum. Meth.* **B5**, p. 430-435.

Lazar, C., E.D. Young, and C.E. Manning, Experimental determination of equilibrium nickel isotope fractionation between metal and silicate from 500°C to 950°C. (2012) *Geochim. Cosmochim. Acta* **86**, p. 276-295.

Lee, T., D.A. Papanastassiou, and G.J. Wasserburg, Demonstration of Mg-26 excess in Allende and evidence for Al-26. (1976) *Geophys. Res. Lett.* **3**, p. 109-112.

Lee, T., D.A. Papanastassiou, and G.J. Wasserburg, Calcium isotopic anomalies in Allende meteorite. (1978) *Astrophys. J.* **220**, L21-L25.

Luck, J.-M., D.B. Othman, J.A. Barrat, and F. Albarède, Coupled ^{63}Cu and ^{16}O excesses in chondrites. (2003) *Geochim. Cosmochim. Acta* **67**, p. 143-151.

Lugmair, G.W. and S.J.G. Galer, Age and isotopic relationships among the angrites Lewis Cliff-86010 and Angra-Dos-Reis. (1992) *Geochim. Cosmochim. Acta* **56**, p. 1673-1694.

Lugmair, G.W. and A. Shukolyukov, Early solar system timescales according to ^{53}Mn-^{53}Cr

systematics. (1998) *Geochim. Cosmochim. Acta* **62**, p. 2863-2886.

Mahon, K. The new "York" regression: application of an improved statistical method to geochemistry. (1996) *Int. Geol. Rev.* **38**, p. 293–303.

Marhas, K., S. Amari, F. Gyngard, E. Zinner, and R. Gallino, Iron and nickel isotopic ratios in presolar SiC grains. (2008) *Astrophys. J.* **689**, p. 622-645.

McCulloch, M.T. and G.J. Wasserburg, Barium and neodymium isotopic anomalies in the Allende meteorite. (1978) *Astrophys. J.* **220**, L15-19.

McCulloch, M.T. and G.J. Wasserburg, More anomalies from the Allende meteorite: samarium. (1978) *Geophys. Res. Lett.* **5**, p. 599-602.

Mishra, R.K., J.N. Goswami, S. Tachibana, G.R. Huss, and N.G. Rudraswami, ^{60}Fe and ^{26}Al in chondrules from unequilibrated chondrites: implications for early solar system processes. (2010) *Astrophys. J.* **714**, p. L217-L221.

Mishra, R.K. and J.N. Goswami, Fe-Ni and Al-Mg isotope records in UOC chondrules: plausible stellar source of ^{60}Fe and other short-lived nuclides in the early solar system. (2014) *Geochim. Cosmochim. Acta* **132**, p. 440-457.

Mishra, R.K. and M. Chaussidon, Fossil records of high level of ^{60}Fe in chondrules from unequilibrated chondrites. (2014) *Earth Planet. Sci. Lett.* **398**, p. 90-100.

Mishra, R.K., K.K. Marhas, and Sameer, Abundance of ^{60}Fe inferred from nanoSIMS study of QUE 97008 (L3.05) chondrules. (2016) *Earth Planet. Sci. Lett.* **436**, p. 71-81.

Morand, P. and C.J. Allègre, Nickel isotopic studies in meteroites. (1988) *Earth Planet. Sci. Lett.* **63**, p. 167-176.

Mostefaoui, S., G.W. Lugmair, P. Hoppe, and A. El Gorsey, Evidence for live ^{60}Fe in meteorites. (2004) *New Astron. Rev.* **48**, p. 155-159.

Mostefaoui, S., G.W. Lugmair, and P. Hoppe, ^{60}Fe: a heat source for planetary differentiation from a nearby supernova explosion. (2005) *Astrophys. J.* **625**, p. 271-277.

Moynier, F., J. Blichert-Toft, P. Telouk, J.-M. Luck, and F. Albarède, Comparative stable isotope geochemistry of Ni, Cu, Zn and Fe in chondrites and iron meteorites. (2007) *Geochim. Cosmchim. Acta* **71**, p. 4365-4379.

Moynier, F., J. Blichert-Toft, K. Wang, G.F. Herzog, and F. Albarède, The elusive ^{60}Fe in the solar system. (2011) *Astrophys. J.* **741**, p. 71.

Niederer, F.R., D.A. Papanastassiou, and G.J. Wasserburg, Endemic isotopic anomalies in titanium. (1980) *Astrophys. J.* **240**, L73-L77.

Niemeyer, S. and G.W. Lugmair, Ubiquitous isotopic anomalies in Ti from normal Allende inclusions. (1981) *Earth Planet. Sci. Lett.* **53**, p. 211-225.

Niemeyer, S. and G.W. Lugmair, Titanium Isotopic Anomalies in Meteorites. (1984) *Geochim. Cosmochim. Acta* **48**, p. 1401-1416.

Ogliore, R.C., G.R. Huss, and K. Nagashima, Ratio estimation in SIMS analysis. (2011) *Nucl. Instrum. Meth. Phys. Res. B* **269**, p. 1910-1918.

Papanastassiou, D.A. and G.J. Wasserburg, Initial strontium isotopic abundances and the resolution of small time differences in the formation of planetary objects. (1969) *Earth Planet. Sci. Lett.* **5**, p. 361-376.

Peacock, C. and D.M. Sherman, Sorption of Ni by birnessite: equilibrium constrols on Ni in seawater. (2007) *Chem. Geol.* **238**, p. 94-106.

Porter, S.J., D. Selby, and V. Cameron, Charcaterising the nickle isotopic composiiton of organic-rich marine sediments. (2014) *Chem. Geol.* **387**, p. 12-21.

Qin, L., L.R. Nittler, C. Alexander, M. O'D, J. Wang, F.J. Staldermann, and R.W. Carlson, Extreme ^{54}Cr-rich nano-oxides in the CI chondrite Orgueil- implication for a late supernova injection into the solar system. (2011) *Geochim. Cosmochim. Acta* **75**, p. 629-644.

Quitté, G., M. Meier, C. Latkoczy, A.N. Halliday, and D. Günther, Nickel isotopes in iron meteorites-nucleosynthetic anomalies in sulfides with no effects in metals and no trace of Fe-60. (2006) *Earth Planet. Sci. Lett.* **242**, p. 16-25.

Quitté, G., and F. Oberlei, Quantitative extraction and high precision isotope measurements of nickel by MC-ICPMS. (2006) *J. Anal. At. Spectrom.* **21**, p. 1249-1255.

Quitté, G., A.N. Halliday, B.S. Meyer, A. Markowski, C. Latkoczy, and D. Günther, Correlated iron 60, nickel 62, and zirconium 96 in refractory inclusions and the origin of the solar system. (2007) *Astrophys. J.* **655**, p. 678-684.

Quitté, G., A. Markowski, C. Latkoczy, A. Gabriel, and A. Pack, Iron-60 heterogeneity and incomlete isotope mixing in the early solar system. (2010) *Astrophys. J* **720**, p. 1215-1224.

Quitté, G., C. Latkoczy, M. Schönbächler, A.N. Halliday, and D. Günther, ^{60}Fe-^{60}Ni systematics in the eucrite parent body: a case study of Bouvante and Juvinas. (2011) *Geochim. Cosmochim. Acta* **75**, p. 7698-7706.

Ratié, G., D. Jouvin, J. Garnier, O. Rouxel, S. Miska, E. Guimarães, L. Cruz Viera, Y. Sivry, I. Zelano, E. Montarges-Pelletier, F. Thil, and C. Quantin, Nickel isotope fractionation during tropical weathering of ultramafic rocks. (2015) *Chem. Geol.* **402**, p. 68-76.

Ratié, G., C. Quantin, D. Jouvin, D. Calmels, V. Ettler, Y. Sivry, L. Cruz Viera, E. Ponzevera, and J. Garnier, Nickel isotope fractionation during laterite Ni ore smelting and refining: implications for tracing the sources of Ni in smelter-affected soils. (2016) *Appl. Geochem.* **64**, p. 136-145.

Regelous, M., T. Elliott, and C.D. Coath, Nickel isotope heterogeneity in the early Solar System. (2008) *Earth Planet. Sci. Lett.* **272**, p. 330-338.

Reynolds, J.H., Determination of the age of the elements. (1960) *Phys. Rev. Lett.* **4**, p. 8-10.

Robbins, L.J., E.D. Swanner, S.V. Lalonde, M. Eickhoff, M.L. Parnich, C.T. Reinhard, C.L. Peacock, A. Kappler, and K.O. Konhauser, Limited Zn and Ni mobility during simulated iron formation diagenesis. (2015) *Chem. Geol.* **402**, p. 30-39.

Rudge, J.F., B.C. Reynolds, and B. Bourdon, The double spike toolbox. (2009) *Chem. Geol.* **265**, p. 420-431.

Rugel, G., T. Faestermann, K. Knie, G. Korschinek, M. Poutivtsev, D. Schumann, N. Kivel, I. Günther-Leopold, R. Weinreich, and M. Wohlmuther, New measurement of the ^{60}Fe half-life. (2009) *Phys. Rev. Lett.* **103**, 072502.

Schiller, M., J. Baker, J. Creech, C. Paton, M.-A. Millet, A.J. Irving, and M. Bizzarro, Rapid timescales for magma ocean crystallisation on the Howardite-Eucrite-Diogenite parent body. (2011) *Astrophys. J.* **740**, p. L22.

Shimamura, T. and G.W. Lugmair, Ni isotopic compositions in Allende and other meteorites. (1983) *Earth Planet. Sci. Lett.* **63**, p. 177-188.

Shukolyukov, A. and G.W. Lugmair, Live iron-60 in the early solar-system. (1993a) *Science* **259**,

p. 1138-1142.

Shukolyukov, A. and G.W. Lugmair, ^{60}Fe in eucrites. (1993b) *Earth Planet. Sci. Lett.* **119**, p. 159-166.

N. Sugiura, A. Miyazaki, and Q.-Z. Yin. Heterogeneous distribution of ^{60}Fe in the early solar nebula: achondrite evidence. *Earth Planets Space*, (2006) **58**, p1079–1086.

Spivack-Birndorf, L.J., M. Wadhwa, and P.E. Janney, ^{60}Fe-^{60}Ni chronology of the d'Orbigny angrite: implications for the initial solar system abundance of ^{60}Fe. (2011) *Lunar Planet. Sci.* **42**, 2281.

Steele, R.C.J., T. Elliott, C.D. Coath, and M. Regelous, Confirmation of mass-independent Ni isotopic variability in iron meteorites. (2011) *Geochim. Cosmochim. Acta* **75**, p. 7906-7925.

Steele, R.C.J., C.D. Coath, M. Regelous, S. Russell, and T. Elliott, Neutron-poor nickel isotope anomalies in meteorites. (2012) *Astrophys. J.* **756**, doi:10.1088/0004-637X/758/1/59.

Steele, R.C.J. and P. Boehnke, Isotopic evidence for the origins of x grains: implications for Solar System isotope anomalies. (submitted) *Astrophys. J.*

Strelow, F.W.E., A.H. Victor, C.R. van Zyl, and C. Eloff, Distribution coefficients and cation exchange behaviour of elements in hydrochloric acid-acetone. (1971) *Anal. Chem.* **43**, p. 870-876.

Tachibana, S. and G.R. Huss, The initial abundance of ^{60}Fe in the solar system. (2003) *Astrophys. J.* **588**, p. L41-L44.

Tachibana, S., G.R. Huss, N.T. Kita, G. Shimoda, and Y. Morishita, ^{60}Fe in chondrites: debris from a nearby supernova in the early solar system? (2006) *Astrophys. J.* **639**, p. L87-L90.

Takeda, H. and A.L. Graham, Degree of equilibration of eucritic pyroxenes and thermal metamorphism of the earliest planetary crust. (1991) *Meteoritics* **26**, p. 129-134.

Tang, H. and N. Dauphas, Abundance, distribution and origin of ^{60}Fe in the solar protoplanetary disk. (2012) *Earth Planet. Sci. Lett.* **359-360**, p. 248-263.

Tang, H. and N. Dauphas, ^{60}Fe-^{60}Ni chronology of core formation in Mars. (2014) *Earth Planet. Sci. Lett.* **390**, p. 264-274.

Tang, H. and N. Dauphas, Low ^{60}Fe abundance in Semarkona and Sahara 99555. (2015) *Astrophys. J.* **802**, p. 22.

Tanimizu, M. and T. Hirata, Determination of natural isotopc variation in nickel using inductively coupled plasma mass spectrometry. (2006) *J. Anal. At. Spectrom.* **21**, p. 1423-1426.

Telus, M., G.R. Huss, R.C. Ogliore, K. Nagashima, and S. Tachibana, Recalculation of data for short-lived radionuclide systems using less-biased ratio estimation. (2012) *Meteorit. Planet. Sci.* **47**, p. 2013-2030.

Telus, M., G.R. Huss, R.C. Ogliore, K. Nagashima, D.L. Howard, M.G. Newville, and A.G. Tomkins, Mobility of iron and nickel at low temperature: implications for the ^{60}Fe-^{60}Ni systematics of chondrules from unequilibrated ordinary chondrites. (2016) *Geochim. Cosmochim. Acta* **178**, p. 87-105.

Touboul, M., P. Sprung, S.M. Aciego, B. Bourdon, and T. Kleine, Hf-W chronology of the eucrite parent body. (2015) *Geochim. Cosmochim. Acta* **156**, p. 106-121.

Trinquier, A., J.L. Birck, and C.J. Allègre, Widespread ^{54}Cr heterogeneity in the inner solar system. (2007) *Astrophys. J.* **655**, p. 1179-1185.

Trinquier, A., J.-L. Birck, C.J. Allègre, C. Göpel, and D. Ulfbeck, ^{53}Mn-^{53}Cr systematics of the early Solar System revisited. (2008) *Geochim. Cosmochim. Acta* **72**, p. 5146-5163.

Trinquier, A., T. Elliott, D. Ulfbeck, C. Coath, A.N. Krot, and M. Bizzarro, Origin of nucleosynthetic isotope heterogeneity in the solar protoplanetary disk. (2009) *Science* **324**, p. 374-376.

Vance, D., S.H. Little, C. Archer, V. Cameron, M. Andersen, M.J.A. Rijkenberg, and T.W. Lyons, The oceanic budgets of nickel and zinc isotopes: the importance of sulfidic environments as illustrated by the Black Sea. (in review) *Phil. Trans. R. Soc. A*.

Ventura, G.T., L. Gall, C. Siebert, J. Prytulak, P. Szatmari, M. Hürlimann, and A.N. Halliday, The stable isotope composition of vanadium, nickel and molybdenum in crude oils. (2015) *Appl. Geochem.* **59**, p. 104-117.

Victor, A.H. Separation of nickel from other elements by cation-exhange chromatography in dimethylglyoxime/hydrochloric acid/acetone media. (1986) *Anal. Chim. Acta* **183**, p. 155-161.

Wahlgren, M., K.A. Orlandini, and J. Korkisch, Specific cation-exchange separation of nickel. (1970) *Anal. Chim. Acta* **52**, p. 551-553.

Walker, R.J., J.W. Morgan, A.J. Naldrett, C. Li, and J.D. Fassett, Re-Os isotope sytematics of Ni-Cu sulfide ores, Sudbury Igneous Complex, Ontario: evidence for a major crustal component. (1991) *Earth Planet. Sci. Lett.* **105**, p. 416-429.

Wang, W., G. Audi, A.H. Wapstra, F.G. Kondev, M. MacCormick, X.S. Xu, and B. Pfeiffer, The AME2012 atomic mass evaluation (II). (2012) *Chinese Phys.* **C36**, p. 1603-2014.

Wasserburg, G.J., R. Gallino, and M. Busso, A test of the supernova trigger hypothesis with Fe-60 and Al-26. (1998) *Astrophys. J.* **500**, p. L189-L193.

Wasylenki, L.E., H.D. Howe, L. Spivak-Birndorf, and D.L. Bish, Ni isotope fractionation during sorption to ferrihydrite: implications for Ni in banded iron formations. (2015) *Chem. Geol.* **400**, p. 56-64.

Weiss, D.J., T.F.D. Mason, F.J. Zhao, G.J.D. Kirk, B.J. Coles, and M.S.A. Horstwood, Isotopic discrimination of zinc in higher plants. (2005) *New Phytol.* **165**, p. 703-710.

Wieser, M.E., N.E. Holden, T.B. Coplen, J.K. Böhlke, M. Berglund, W.A. Brand, P. de Bièvre, M. Gröning, R.D. Loss, J. Meija, T. Hirata, T. Prohaska, R. Schoenberg, G. O'Connor, T. Walczyk, S. Yoneda, and X.-K. Zhu, Atomic weights of the elements 2011 (IUPAC Technical Report). (2013) *Pure Appl. Chem.* **85**, p. 1047-1078.

Yurimoto, H. and K. Kuramoto, Molecular cloud origin for the oxygen isotope heterogeneity in the solar system. (2004) *Science* **305**, p. 1763-1766.

York, D. Least squares fitting of a straight line with correlated errors. (1969) *Earth and Planet. Sci. Lett*.. **5**, p. 320–324.

TABLE AND FIGURE CAPTIONS

Table 1 Ni isotopic abundances (Gramlich et al. 1989), nuclide masses (Wang et al., 2012) and atomic weight (Wieser et al., 2013).

Table 2 Averages of mass-dependent and mass-independent Ni isotope compositions for meteorites and terrestrial reservoirs. Averages are weighted means and uncertainties of 2 SE_w of multiple analyses unless indicated with * which denotes arithmetic mean uncertainty of 2 SD_w. The weighted mean is the preferred estimator of central tendency when data have differing uncertainties, as in the case of combining different studies. The weighted standard error has been estimated using the expression, $SE_w = \sqrt{\frac{1}{\Sigma_i^n \sigma_i^{-2}}}$. The weighted standard deviation is given by, $SD_w = \sqrt{\frac{\Sigma w_i (x_i - \bar{x})^2}{(N-1)\Sigma w_i n^{-1}}}$. Both the SE_w and SD_w have been adjusted by multiplying by the expression $1 + \frac{1}{4(n-1)}$ which compensates for the bias in standard deviation (and consequently standard error) of small sample sizes (Gurland and Tripathi 1971). Data sources indicated as follows: [A] Birck and Lugmair (1988) [b] Cameron et al. (2009) [c] Cameron and Vance (2014) [D] Chen et al. (2009) [e] Chernonozhkin et al. (2015) [f] Chernonozhkin et al. (2016) [G] Cook et al. (2006) [H] Cook et al. (2006) [I] Cook et al. (2008) [J] Dauphas et al. (2008) [k] Estrade et al. (2015) [l] Gall et al. (2013) [m] Gueguen et al. (2013) [n] Kita et al. (1998) [o] Porter et al. (2014) [P] Quitt´e et al. (2011) [Q] Quitt´e et al. (2006) [R] Quitt´e et al. (2007) [s] Rati´e et al. (2015) [T] Regelous et al. (2008) [U] Shukolyukov and Lugmair (1993a) [V] Shukolyukov and Lugmair (1993b) [W] Steele et al. (2011) [X] Steele et al. (2012) [Y] Tang and Dauphas (2012) [Z] Tang and Dauphas (2014) [AA] Tang and Dauphas (2015) [AB] Tanimizu and Hirata (2006)

Figure 1. Mass independent nickel isotope data for meteorites and CAIs from earlier studies, (a) $\varepsilon^{60}Ni_{58/61}$ vs. $\varepsilon^{62}Ni_{58/61}$ and (b) $\varepsilon^{64}Ni_{58/61}$ vs. $\varepsilon^{62}Ni_{58/61}$. Data from Birck and Lugmair 1988; Cook et al. 2006, 2008; Quitté et al. 2006, 2007. The dashed line indicates the vector of change in composition (from the origin) as a result of error or interference (moving to the lower left) in ^{61}Ni. Some scatter appears to be along this trajectory. For ready comparison with the higher precision data, the blue boxes indicate the dimensions of parameter space shown in Figure 4. An extrapolation of a least squares York regression and the 2σ uncertainty error envelope (York 1968; Mahon 1995) through the bulk meteorite data of Steele et al. 2012 and Tang and Dauphas (2012, 2014) from the origin through the CAI data (see Fig. 4) is shown in Figure 1b for reference.

Figure 2. Mass independent nickel isotope data of sulfide inclusions from iron meteorites (Quitté et al. 2006; Cook et al. 2008; Chen and Papanastassiou., 2009), (a) $\varepsilon^{60}Ni_{58/61}$ vs. $\varepsilon^{62}Ni_{58/61}$ and (b) $\varepsilon^{64}Ni_{58/61}$ vs. $\varepsilon^{62}Ni_{58/61}$. Again the dashed line indicates trajectories caused by error or interference (moving to the lower left) on ^{61}Ni. It appears that ^{61}Ni error may be a dominant (but not sole) cause of variability in the highly anomalous sulfides. The blue boxes indicate the dimensions of parameter space shown in Figure 4.

Figure 3. Mass independent nickel isotope data a) $\varepsilon^{60}Ni_{58/61}$ vs. $\varepsilon^{62}Ni_{58/61}$ and b) $\varepsilon^{64}Ni_{58/61}$ vs. $\varepsilon^{62}Ni_{58/61}$ of bulk meteorite analyses from 'second generation' studies (Dauphas et al., 2008; Regelous et al., 2008; Chen and Papanastassiou, 2009). The samples of Regelous et al. 2008 show small but resolved anomalies in both chondritic and iron meteorites. These analyses are consistent with the less precise data of Dauphas et al. (2008), who conversely argued against bulk Ni isotopic variability (as did Chen and Papanasstiou, 2009). Lines representing ^{61}Ni error and best fit array of Steele et al. (2012) and Tang and Dauphas (2012, 2014) as discussed in caption

to Figure 1. Again (dashed) blue boxes indicate the dimensions of parameter space shown in Figure 4.

Figure 4. Mass independent Ni isotope measurements a) $\varepsilon^{60}Ni_{58/61}$ vs. $\varepsilon^{62}Ni_{58/61}$ and b) $\varepsilon^{64}Ni_{58/61}$ vs. $\varepsilon^{62}Ni_{58/61}$ on bulk meteorites from the highest precision studies (Steele et al., 2011, 2012;Tang and Dauphas, 2012, 2014). Data from these studies show a consistent set of anomalies between carbonaceous, ordinary and enstatite chondrites and different groups of iron meteorites. There is a strong positive correlation between $\varepsilon^{62}Ni_{58/61}$ and $\varepsilon^{64}Ni_{58/61}$ with a slope of 3.003 ±0.116 (fitted as described in the caption to Figure 1, and illustrated with black line and grey error envelope), first identified by Steele et al. (2012) and confirmed by Tang and Daphaus (2012). This is array quite distinct from the dashed ^{61}Ni error line.

Figure 5 Plot of $\varepsilon^{64}Ni_{58/61}$ vs $\varepsilon^{50}Ti_{47/49}$ for bulk meteorites (Ti isotope data from Trinquier et al. 2009, Ni data from Steele et al 2012 and Birck and Lugmair 1988). A linear array is defined by analyses of ordinary, enstatite and CI chondrites and this extends intersect with CAI compositions. However, CAI-rich meteorite groups (CV CO) plot above the array, likely reflecting analyses of unrepresentative sub-samples of these meteorites with an excess of CAI ~3-4% by mass (illustrated with a mixing curve from a CI composition). The high Ti/Ni CAIs mean mixing trajectories with bulk chondrite compositions are highly convex up. Thus simple mixing between CAIs and ordinary chondrites (black curve) cannot explain the straight bulk meteorite array.

Figure 6. Representative isochron diagrams for the ^{60}Fe-^{60}Ni system measured by different analytical techniques. (a) TIMS Isochron of different bulk samples of the eucrite Chervony Kut (Shukolyukov and Lugmair 1993a). (b) MC-ICPMS Isochron of mineral separates from the quenched angrite D'Orbigny (Tang and Dauphas 2012). (c) SIMS Isochron of a single Efremovka chondrule (Ch 1), Mishra and Chaussidon (2014). Also shown are recalculated least squares linear York regressions (York 1968, Mahon 1995) for each dataset, yielding $^{60}Fe/^{56}Fe°$. Note the highly contrasting values obtained by bulk (a) and (b) versus *in situ* analysis (c) for objects of comparable age.

Figure 7. A plot of the evolution of Co/Ni (expressed as $^{59}Co/^{60}Ni$) and Fe/Ni (as $^{56}Fe/^{58}Ni$) with fractional (Rayleigh) crystallisation of a model chondrule. The values shown are for an olivine crystal that is grown from the evolving melt. We have used representative partition coefficients from Gaetani and Grove (1995), $D(Ni)_{olivine\text{-}melt} = 5.9$, $D(Co)_{olivine\text{-}melt} = 1.96$ $D(Ni)_{olivine\text{-}melt} = 0.916$ and $D(Ni)_{sulfide\text{-}melt} = 510$, $D(Co)_{sulfide\text{-}melt} = 17.7$, $D(Fe)_{sulfide\text{-}melt} = 1.53$. We assume the chondrule starts with chondritic elemental abundances [Ni]=10500ppm, [Co]=500 ppm, [Fe]= 181000ppm and crystallises only olivine and sulfide. Since sulfide has a strong influence on partitioning, we show cases with masses of (modally) crystallising sulfide at the low (0.2%) and high (1%) ends of the ranges of troilite abundances in chondrules reported by Jones (1990). Tick marks represent 0.12, 0.14, 0.16 and 0.18 solid fractionation for the high sulfide case and 0.35, 0.4, 0.45 and 0.5 for the low sulfide case. Also shown are two points at the high Fe/Ni end of isochrons from two chondrule analysed by SIMS (Mishra and Chaussidon 2014). The values of these two points on the y-axis correspond to the $^{59}Co/^{60}Ni$ required to explain their associated $^{60}Ni/^{58}Ni$ anomaly by $^{59}CoH^+$ interference alone. This value is calculated assuming $^{59}CoH/^{59}Co$ production is the same as $^{56}FeH/^{56}Fe$ reported in Mishra and Chaussidon (2014) and the $^{59}Co/^{60}Ni$ calculated at requisite $^{56}Fe/^{58}Ni$. The range reported reflects the different $^{59}Co/^{60}Ni$ calculated using the two values for $^{56}FeH/^{56}Fe$ evident in the appendix of Mishra and Chaussidon (2014) and includes the error reported on the $^{60}Ni/^{58}Ni$. One of the ^{60}Ni anomalies (Ch12), and much of the other (Ch1), can be entirely explained by $^{59}CoH^+$ according to these calculations, although more work is required to constrain better all input values.

Figure 8. Mass-dependent Ni isotope data, $\delta^{60/58}$Ni for different geochemical reservoirs. Data for (a) bulk meteorites (Cameron et al., 2009; Chernonozhkin et al., 2015, 2016; Gueguen et al.,

2013; Moynier et al., 2007; Steele et al., 2011, 2012), (b) terrestrial igneous rocks and Ni ores, formed by sulfide segregation in igneous systems (Cameron et al., 2009; Chernonozhkin et al., 2015; Gueguen et al., 2013; Rati´e et al., 2015; Steele et al., 2011, 2012; Tanimizu and Hirata,
1445 2006). (c) the ocean and major input and output fluxes (Cameron and Vance, 2014; Gall et al., 2013; Gueguen et al., 2013)and (d) biosphere processed materials (Cameron et al., 2009; Estrade et al., 2015; Gueguen et al., 2013; Porter et al., 2014; Rati´e et al., 2015)

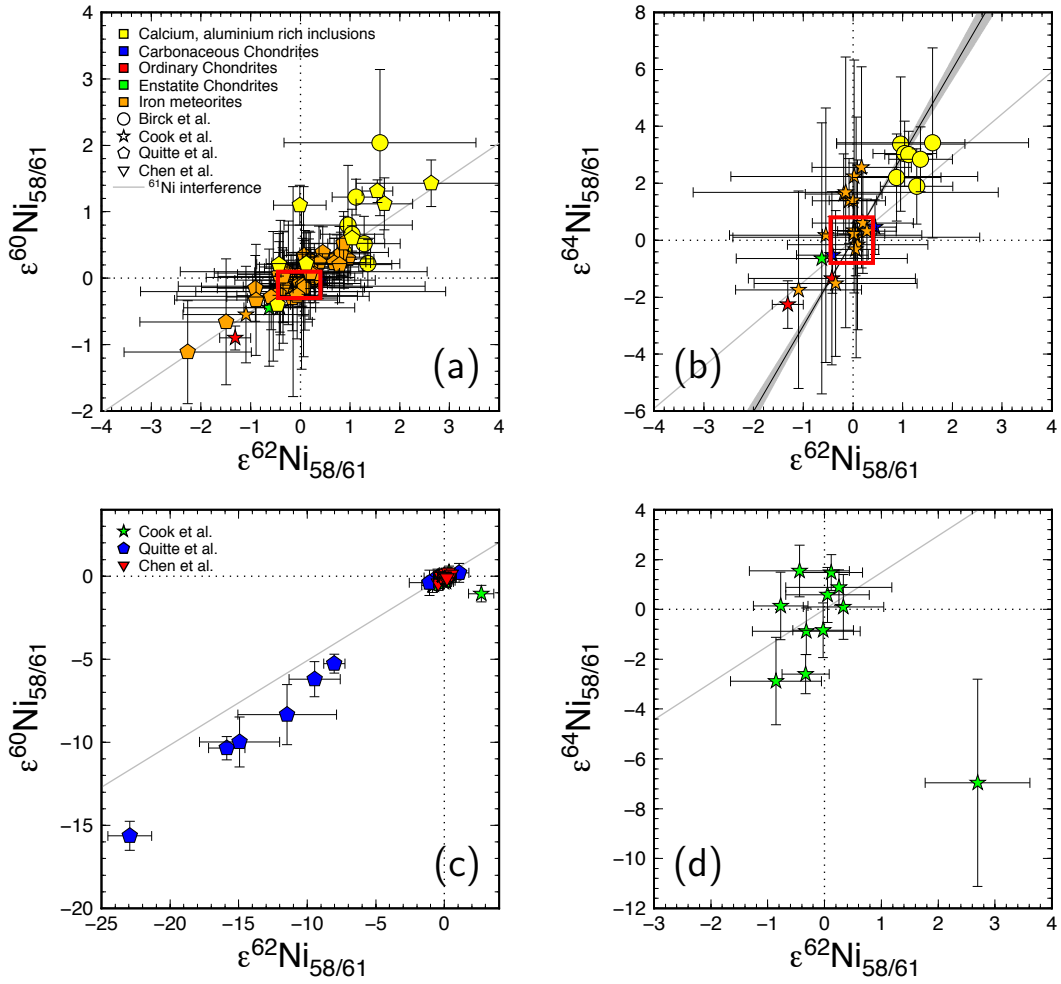
Calcium, aluminium rich inclusions
Carbonaceous Chondrites
Ordinary Chondrites
Enstatite Chondrites
Iron meteorites
Birck et al.
Cook et al.
Quitte et al.
Chen et al.
61Ni interference
(a)
(b)
(c)
(d)
ε60Ni58/61
ε62Ni58/61
ε64Ni58/61

Fig 1

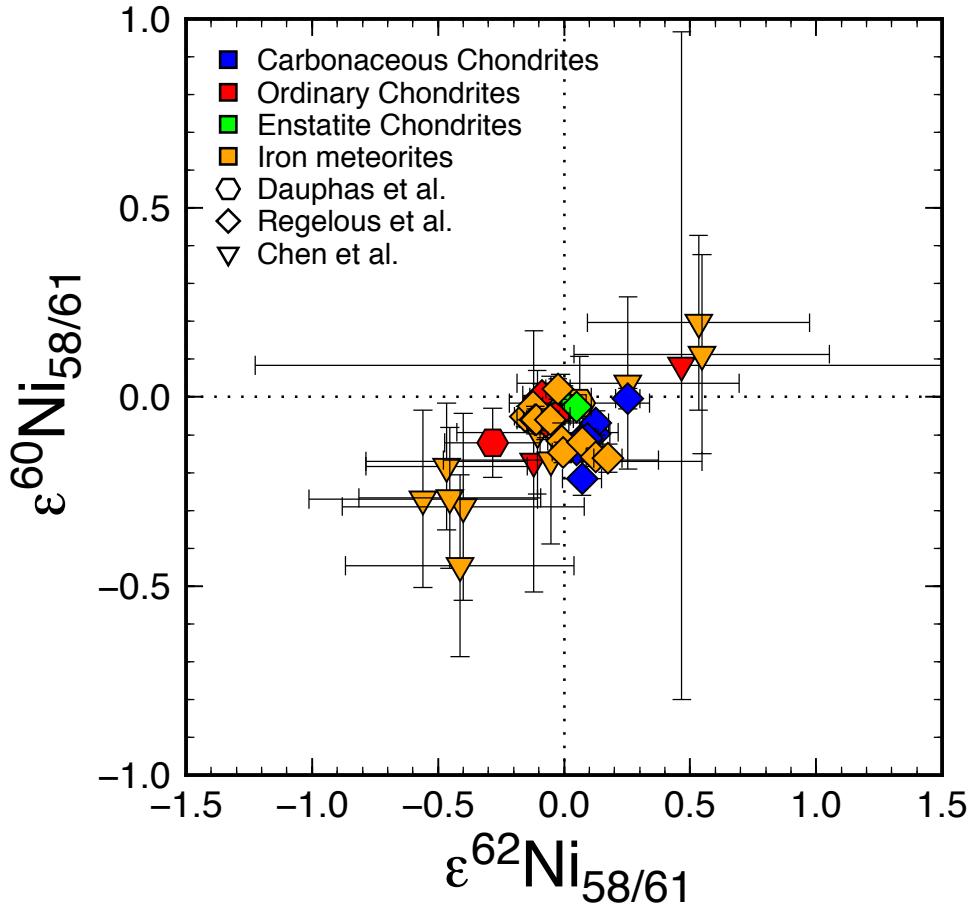
Carbonaceous Chondrites
Ordinary Chondrites
Enstatite Chondrites
Iron meteorites
Dauphas et al.
Regelous et al.
Chen et al.
1.0
0.5
0.0
−0.5
−1.0
−1.5
−1.0
−0.5
0.0
0.5
1.0
1.5
ε60Ni58/61
ε62Ni58/61

Fig 2

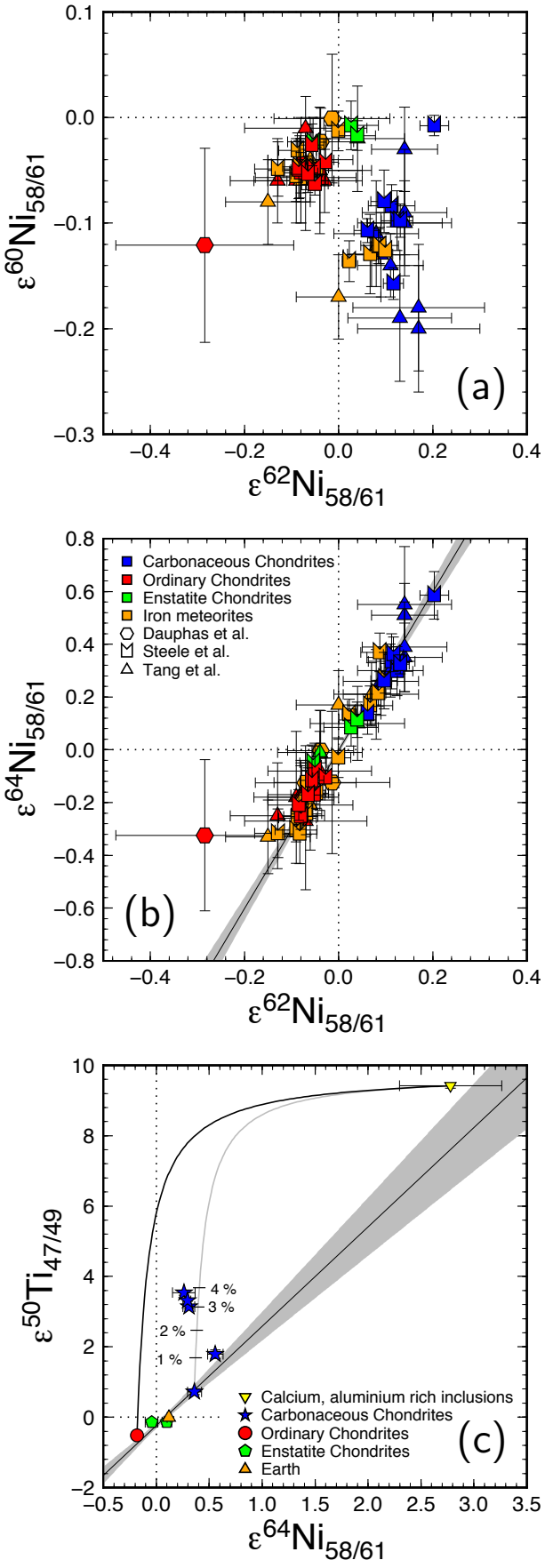
(a)
$\varepsilon^{60}Ni_{58/61}$
$\varepsilon^{62}Ni_{58/61}$
(b)
Carbonaceous Chondrites
Ordinary Chondrites
Enstatite Chondrites
Iron meteorites
Dauphas et al.
Steele et al.
Tang et al.
$\varepsilon^{64}Ni_{58/61}$
$\varepsilon^{62}Ni_{58/61}$
(c)
4 %
3 %
2 %
1 %
Calcium, aluminium rich inclusions
Carbonaceous Chondrites
Ordinary Chondrites
Enstatite Chondrites
Earth
$\varepsilon^{50}Ti_{47/49}$
$\varepsilon^{64}Ni_{58/61}$

Fig 3

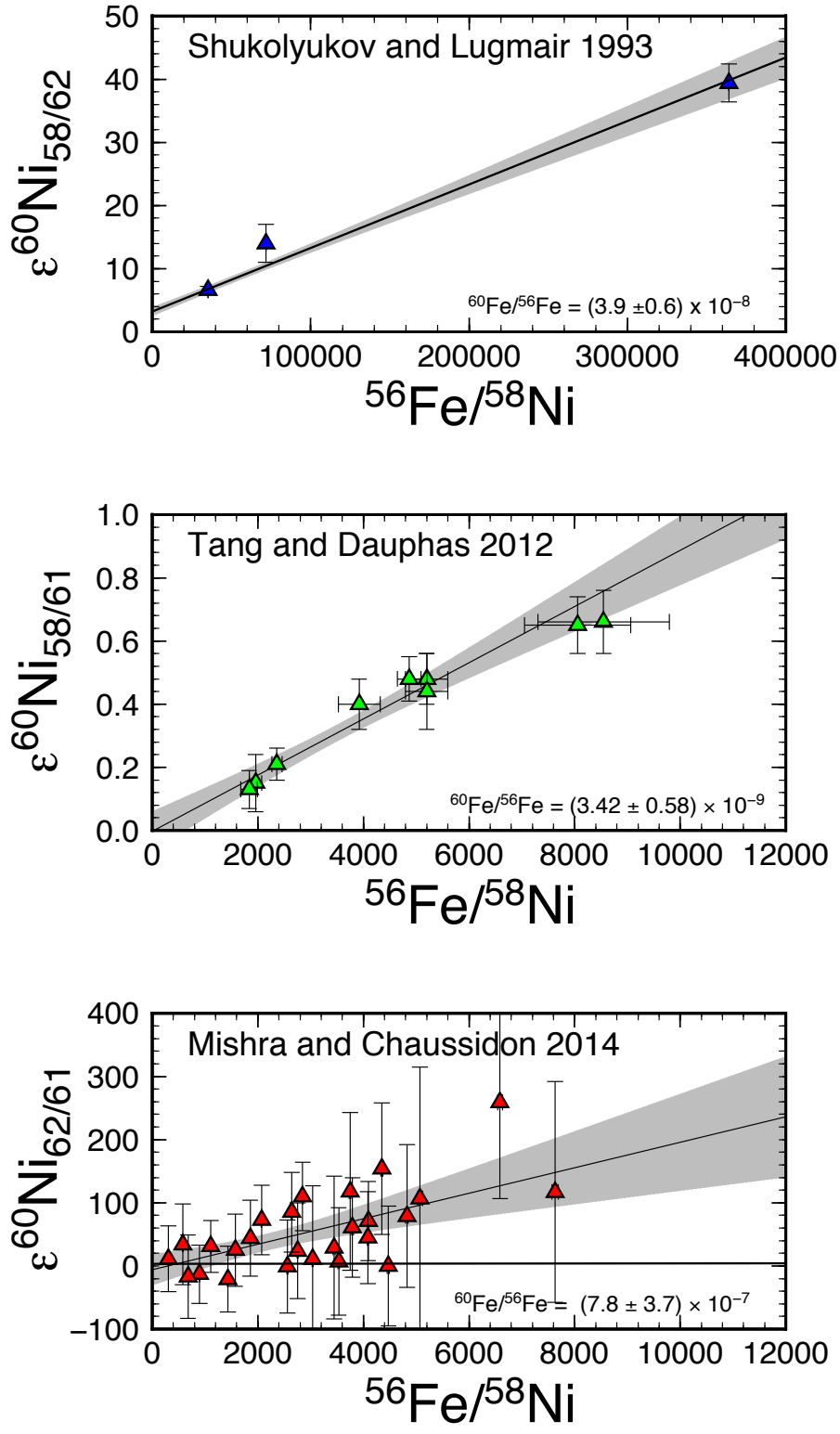
Shukolyukov and Lugmair 1993
$^{60}Fe/^{56}Fe = (3.9 \pm 0.6) \times 10^{-8}$
$\varepsilon^{60}Ni_{58/62}$
$^{56}Fe/^{58}Ni$
Tang and Dauphas 2012
$^{60}Fe/^{56}Fe = (3.42 \pm 0.58) \times 10^{-9}$
$\varepsilon^{60}Ni_{58/61}$
$^{56}Fe/^{58}Ni$
Mishra and Chaussidon 2014
$^{60}Fe/^{56}Fe = (7.8 \pm 3.7) \times 10^{-7}$
$\varepsilon^{60}Ni_{62/61}$
$^{56}Fe/^{58}Ni$

Fig 4

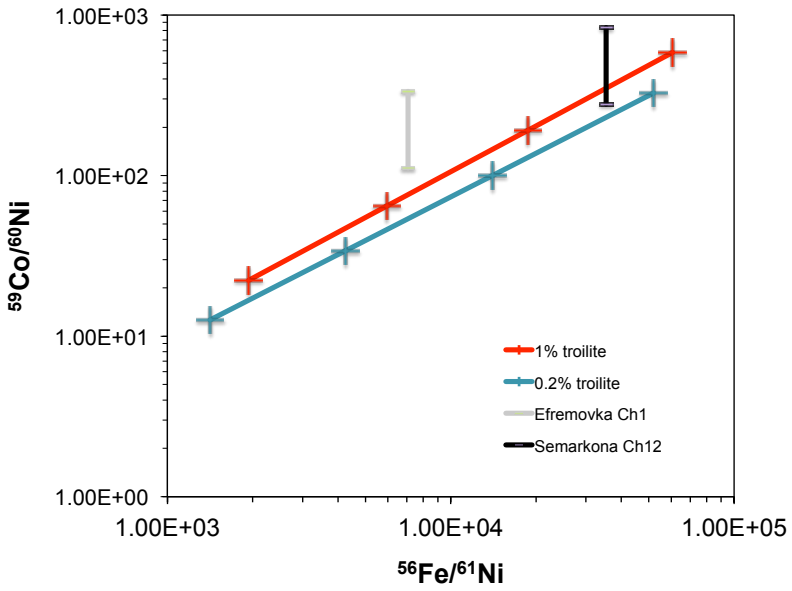
1.00E+03
1.00E+02
1.00E+01
1.00E+00
59Co/60Ni
1.00E+03
1.00E+04
1.00E+05
56Fe/61Ni
1% troilite
0.2% troilite
Efremovka Ch1
Semarkona Ch12

Fig 5

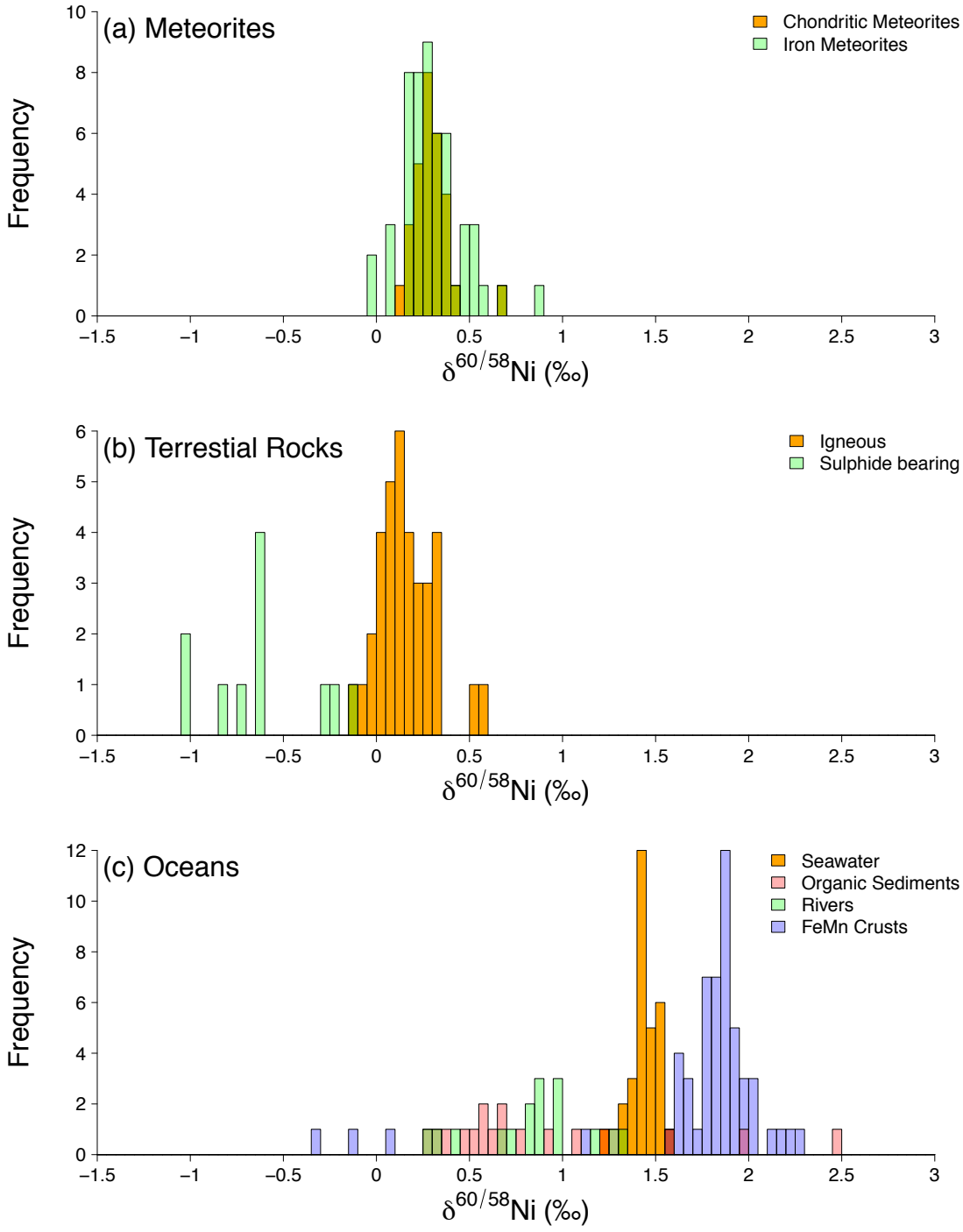
(a) Meteorites
Chondritic Meteorites
Iron Meteorites
Frequency
δ60/58Ni (‰)
(b) Terrestial Rocks
Igneous
Sulphide bearing
Frequency
δ60/58Ni (‰)
(c) Oceans
Seawater
Organic Sediments
Rivers
FeMn Crusts
Frequency
δ60/58Ni (‰)

1450 Fig 6